

TWEEQU THERMOBAROMETRY: ANALYSIS OF UNCERTAINTIES AND APPLICATIONS TO GRANULITES FROM WESTERN ALASKA AND AUSTRIA

JOSHUA LIEBERMAN*

Mineralogisch-petrographisches Institut, Universität Bern, Baltzerstrasse 1, CH-3012 Bern, Switzerland

KONSTANTIN PETRAKAKIS

Institut für Petrologie, Universität Wien, Dr. Karl Lüger-Ring 1, A-1010 Wien, Austria

ABSTRACT

Calculation of all possible equilibria involving minerals of a metamorphic paragenesis yields several advantages for thermobarometry over the use of a single thermometer with a single barometer. The advantages can only be realized where thermobarometric calculations are based on an internally consistent thermodynamic data-set for the minerals of interest and where three or more of the applicable equilibria are linearly independent. This report considers the quality of pressures and temperatures of equilibration estimated in this manner by analyzing the systematic departure of equilibria from a single mutual P-T intersection. Limiting uncertainties in pressures and temperatures due to imprecision in mineral analyses are calculated by means of a Monte Carlo simulation. This serves as a general model for the analysis of thermobarometric uncertainties, for which analytical parametric methods of error propagation typically are not appropriate. Calculations are presented for several garnet - pyroxene gneisses from the Kigluaik Mountains, western Alaska, and the Bohemian Massif, Austria. Examination of subsets of the possible equilibria for two Kigluaik samples shows that scatter of the P-T intersections is most likely due in one case to the easy perturbability of low-entropy (or low-volume) equilibria, and in the other to retrograde re-equilibration. Observed and simulated variations in mineral compositions lead to comparable uncertainties in the P-T determination for one Bohemian sample. Confidence regions in P-T space derived by Monte Carlo simulation demonstrate that the use of all possible equilibria together in a TWEEQU analysis yields a much less uncertain P-T estimate than the use of any arbitrary single thermobarometer pair.

Keywords: metamorphism, thermobarometry, error analysis, Monte Carlo, Seward Peninsula, Alaska, Moldanubia, Austria.

SOMMAIRE

Un calcul de tous les équilibres possibles parmi les minéraux d'une paragenèse métamorphique s'avère beaucoup plus profitable pour une analyse thermobarométrique qu'une considération d'un seul géothermomètre et d'un seul géobaromètre. Les avantages deviennent apparents seulement si les calculs thermobarométriques sont fondés sur une banque de données pour les minéraux pertinents à compatibilité interne, et si trois équilibres ou plus font preuve d'une indépendance linéaire. Nous considérons ici la qualité des valeurs de pression et de température d'équilibrage estimées de cette façon en analysant l'écart systématique des équilibres d'une seule intersection P-T commune. Les incertitudes limitantes en pression et en température dues à l'imprécision dans les compositions des minéraux ont été calculées par simulation de Monte Carlo. Ceci sert de modèle général pour l'analyse des incertitudes thermobarométriques; une propagation des erreurs par méthodes paramétriques et analytiques n'est généralement pas appropriée à ces cas. Nos calculs ont été faits pour plusieurs exemples de gneiss à grenat - pyroxène des montagnes Kigluaik, dans l'Alaska occidentale, et dans le massif bohémien, en Autriche. L'examen de sous-assemblages des équilibres possibles dans le cas de deux échantillons de Kigluaik montre que l'écart des intersections P-T est tout probablement dû dans un cas à la facilité avec laquelle les équilibres à faible entropie (ou faible volume) peuvent être perturbés, et dans l'autre au ré-équilibrage rétrograde. Dans la détermination de P et T pour un échantillon bohémien, les incertitudes dues aux variations réelles et simulées dans la composition des minéraux sont comparables. Les limites de confiance en termes de P et T dérivées de la simulation de Monte Carlo démontrent que l'utilisation simultanée de tous les équilibres possibles dans une analyse au moyen du logiciel TWEEQU donne une incertitude dans l'estimation des conditions P-T moins grande que ne résulterait de l'usage de n'importe quelle paire d'indicateurs thermométrique et barométrique.

(Traduit par la Rédaction)

Mots-clés: métamorphisme, thermobarométrie, analyse d'erreurs, Monte Carlo, péninsule de Seward, Alaska, Moldanubie, Autriche.

*Present address: Institute of Earth Sciences, Hebrew University, Givatram, 91904 Jerusalem, Israel.

INTRODUCTION

The estimation of the temperatures and pressures under which metamorphic rocks formed is an important goal of modern petrology. Such estimates are necessary both for an understanding of the chemistry and physics of metamorphic processes, and for a derivation of the constraints on the tectonic processes responsible for metamorphism. Equally important is an evaluation of the uncertainties, in both relative and absolute senses, attached to derived P-T values (Hodges & Crowley 1985, Hodges & McKenna 1987, Kohn & Spear 1991, Powell 1985).

There are several methods of P-T estimation in use, with various presumed degrees of reliability. These include geological reasoning, interpretation of textures in light of a petrogenetic grid, direct experimental studies, inference from a calculated phase-diagram, or use of calibrated geothermometers and geobarometers. Whether implicit or explicit, quantitative or qualitative, all of these methods reduce in essence to one: experimental calorimetric or phase-equilibrium studies or both are extrapolated by means of a theoretical or empirical model to interpret the equilibrium phase-relations applicable to a particular metamorphic bulk-composition. Three critical conditions for successful interpretation of P-T conditions are:

- 1) Some form of instantaneous thermodynamic equilibrium has been *achieved* and *preserved* within the natural rock sample.
- 2) The extrapolation from experimental studies to the thermodynamic properties of natural minerals has been *correctly* accomplished.
- 3) The analyzed mineral compositions are *perfect*.

Any valid method of deriving confidence limits on P-T estimates must test the applicability of these assumptions to each rock studied.

This report concerns the application of a general method of P-T estimation: Thermobarometry With Estimation of EQUilibration state (TWEEQU) (Berman 1991). Beginning with an internally consistent thermodynamic data-base (Berman 1988, Berman *et al.* 1985), all possible equilibria among minerals of a given metamorphic paragenesis are simultaneously considered (Berman *et al.* 1987). TWEEQU makes an explicit and internally consistent extrapolation, including the use of P-T-dependent activity models, from experimental phase-equilibrium data to a natural paragenesis. It allows in many cases an evaluation of the degree to which the three conditions above have been fulfilled.

Imprecision in the input data, such as the analyzed compositions of minerals, places important limits on the precision with which a pressure and temperature can be known, even if the first

two conditions for thermobarometry are perfectly met. For some parts of the calculation procedure, the confidence regions in P and T resulting from this imprecision could be derived by the standard method for propagation of errors. For other parts, this is neither desirable nor possible. Under such circumstances, the only applicable method of error propagation is a Monte Carlo simulation (Anderson 1976). TWEEQU and Monte Carlo techniques are discussed below as they pertain to reliability in thermobarometry, followed by their application to metamorphic rocks from two high-grade terranes. A Monte Carlo simulation is employed to investigate both the magnitude and shape of confidence regions in P and T for reasonable errors in microprobe analyses. Use of simulation techniques to express and apply uncertainties derived from thermochemical data will be described in a subsequent report.

METHODS

TWEEQU thermobarometry

The basic thermobarometer consists of two intersecting mineral equilibria with different P-T slopes. The equilibria are displaced in P-T space from their nominal positions according to the activities of the mineral species involved in the equilibria, calculated from the analyzed compositions of minerals in an inferred metamorphic paragenesis. No matter how the two equilibria are displaced, they will by definition intersect somewhere, at some point in P-T space. The reliability of this point can be judged to some extent on the basis of geological reasoning. For example, several samples collected within a small area should give similar results (Lieberman & Rice 1986), samples from a traverse along a metamorphic gradient should give a smooth range of temperatures (Chipera & Perkins 1988), or resulting pressures should agree with aluminosilicate occurrences (Hodges & Spear 1982). In some cases, however, the test of thermobarometry is simply how well it agrees with preconceived notions of acceptable results.

The minerals in a metamorphic paragenesis can generally be related to one another by three or more different simultaneous equilibria among mineral species. This opens the possibility of generating three or more mutual P-T intersections and comparing their relative closeness as a measure of reliability. Note, however, that if the set of equilibria contains only two linearly independent equilibria, then all the equilibria will be algebraically constrained to intersect in a single P-T point (excluding mirror invariant points). This will be

true no matter what thermochemical data, or activities, are used for the minerals involved, as long as the same values are used to calculate each equilibrium. Conversely, the failure of such a set of equilibria to converge in a point provides no test of P-T reliability, but only indicates internal inconsistency in the calculation (Berman 1991).

If three or more linearly independent equilibria can be applied to a single paragenesis, on the other hand, no such algebraic constraint applies. As long as all equilibria are calculated from a single, internally consistent set of thermodynamic data (this includes consistent activity-composition models and equations of state), then the distribution of mutual P-T intersections among the equilibria will truly be a measure of the reliability of the P-T determination in the sense of all three necessary conditions for reliability: preservation of equilibrium in the sample, natural validity of the thermodynamic model, and analytical accuracy. Since the intersection of any two possible equilibria, whether invariant or indifferent, stable or metastable (in the sense of a Schreinemaker diagram), is a potentially correct P-T determination, it is also important that all equilibria be calculated, not just a linearly independent subset of equilibria, and that P- or T-dependent activity coefficients be calculated anew for each different combination of P and T (Berman 1991).

Not only will the extent to which P-T intersections are dispersed from one another give a measure of the reliability of the P-T determination, but also the pattern of dispersion may in some cases give an indication of where the problem lies and which condition for reliability has been most seriously violated. This type of interpretation is illustrated below by the examination of subsets of equilibria that exclude particular minerals or mineral species. The resulting diagrams are considered in light of petrographic evidence and the likely effects of metamorphic processes such as slow cooling, as well as the likely sensitivity of particular equilibria to imprecise or inaccurate data.

Monte Carlo simulation

In order to estimate the precision of P-T determinations, one needs a way of propagating input uncertainties through the entire TWEEQU calculation. In general, given a vector-valued function $F(\mathbf{x}) = \mathbf{y}$, the basic equation for deriving the variance-covariance matrix $V(\mathbf{y})$ of the output variables $\{y_1, y_2, y_3, \dots, y_n\}$ from the variance-covariance matrix $V(\mathbf{x})$ of an input dataset $\{x_1, x_2, x_3, \dots, x_n\}$ is the following (Bevington 1969, Powell 1985):

$$V(\mathbf{y}) = \mathbf{J}V(\mathbf{x})\mathbf{J}^T \quad (1)$$

where J is the Jacobian matrix of F : $J_{ij} = \frac{\partial F_j(x_i)}{\partial x_i}$

There are three difficulties in implementing this approach. First, the partial derivatives of a complicated function may be difficult or impossible to calculate. This difficulty can be skirted at some computational cost by using finite difference approximations to the Jacobian matrix (Roddick 1987).

A further difficulty, however, is that the equation above, which is properly the first term of a Taylor expansion about the mean \mathbf{x} , is only exact for linear functions. It may or may not be a good approximation for nonlinear functions, depending on the nature of the nonlinearity and the magnitude of the variance in \mathbf{x} . Roddick (1987) offered some procedures to test whether the linear approximation is a good one in specific cases. A third difficulty is encountered in cases where some nonlinear function $F(\mathbf{x})$ results in \mathbf{y} with a different distribution or rank than \mathbf{x} . For example, a function may map normally distributed \mathbf{x} onto non-normally distributed \mathbf{y} . The propagation equation above provides information on neither the resulting distribution, nor the total covariance structure of \mathbf{y} (Aitchison 1986). In the case where techniques of mathematical programming are used to derive and test thermodynamic data (Berman *et al.* 1986), mathematical techniques have been developed, such as stochastic optimization (Ermoliev & Wets 1988), to allow uncertainty in the input data, but no analytical techniques currently exist to propagate input uncertainties through to the final optimized parameters.

All three difficulties are encountered in a TWEEQU calculation. Particularly where nonideal solution models are used, the equations involved are nonlinear and difficult to differentiate, to a degree that varies with each different calculation. Using finite difference approximations, each possible equilibrium would need to be calculated 8-10 times in order to test the validity of the standard error equation. Even the first and simplest step of calculating a mineral formula by normalizing results of a microprobe analysis adds correlation among elements to the uncorrelated, gaussian distributions of X-ray counting uncertainties (Aitchison 1986, Chayes 1960, Rock 1988). This problem is illustrated in Table 1. Counting uncertainties have been simulated by generating 100 uncorrelated, normally distributed permutations of a garnet composition. The resulting atoms per formula unit (p.f.u.) are strongly correlated (and have non-gaussian distributions), in contrast to the permutations on the analytical data themselves.

TABLE 1. MONTE CARLO SIMULATION OF UNCERTAINTY IN A GARNET COMPOSITION

Sample SL40	Si	[4]Al	[6]Al	Ti	Fe ³⁺	Fe ²⁺	Mn	Mg	Ca
Original Analysis	2.982	0.018	1.973	0.003	0.027	1.524	0.139	0.649	0.691
Mean (100 permutations)	2.98	0.02	1.97	0.003	0.031	1.52	0.139	0.65	0.69

(simulation of 1% relative uncorrelated standard deviation in oxide wt.%)

Variance-covariance matrix for 100 permutations (absolute x 100)

	Si	[4]Al	[6]Al	Ti	Fe ³⁺	Fe ²⁺	Mn	Mg	Ca
Si	3.2	-2.9	1.1	0	-1.8	0	-0.12	-0.34	-0.65
[4]Al		2.6	-1.1	0	1.7	-0.14	0.11	0.33	0.35
[6]Al			2	0	-2.2	0.67	0	-0.36	-0.54
Ti				0	0	0	0	0	0
Fe ³⁺					2.5	-0.68	0.11	0.44	0.67
Fe ²⁺						0.99	0	-0.39	-0.41
Mn							0	0	0
Mg								0.39	0
Ca									0.57

Since any "true" composition adds up by definition to one, this problem of closure or normalization affects any expression of variation in mineral compositions that does not result from counting uncertainty.

With the technique of Monte Carlo simulation (Anderson 1976), these difficulties can be avoided. One simulates, by random sampling of the probability distribution for chosen input-variables, the range of input data that *might* have been obtained, for example through duplicate microprobe analyses. In effect, a population of input data-sets is produced (Fig. 1). The technique is no longer limited to uncorrelated input-variables, as stated by Anderson (1976) and Hodges & McKenna (1987). Virtually any desired variance-covariance matrix for any desired distribution can also be randomly sampled, as long as one has an analytical expression for the distribution (Rubinstein 1981). If one takes the approach of Hodges & McKenna (1987) and analyzes a number of points across a sample in order to define the compositional uncertainty, even the problem of defining a distribution for closed data can be avoided simply by taking random samples from the lists of analytical data themselves, rather than from

Monte Carlo Simulation of Analytical Uncertainties

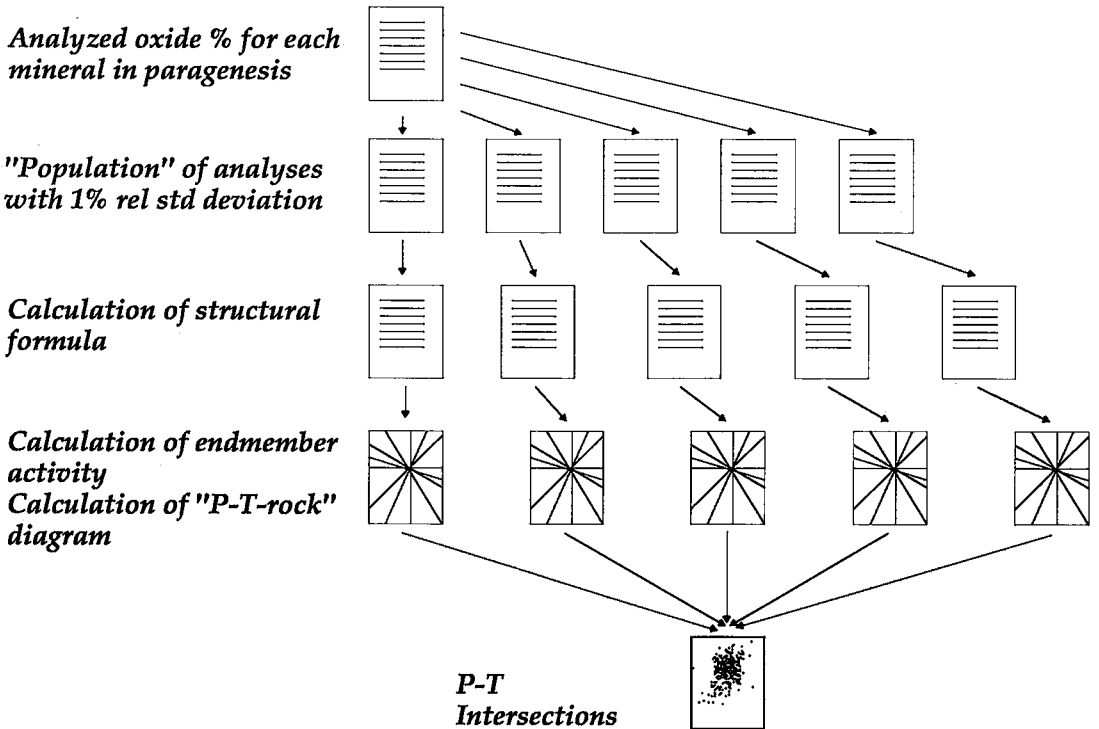


FIG. 1. Schematic diagram of a Monte Carlo simulation. A gaussian error distribution ($1\sigma = 1\%$ relative) is randomly sampled to produce a simulated population of 100 sets of electron-microprobe analyses for a mineral paragenesis. Each set is used separately to calculate a P-T-rock plot: all intersections from every plot are then collected to express the uncertainty in P-T determination.

a distribution that has been fitted arbitrarily to those analytical data.

Each permutation of the input data is used in turn to produce a set of output data, such as values of P and T. The resulting population of output data is an accurate representation in magnitude, distribution, and correlation of the effect of the input uncertainties. At the very least, a Monte Carlo simulation can be used in particular cases to test the validity of the standard method of error propagation. Whereas it is usually a computationally intensive procedure, simulation of a calculation such as TWEEQU is now fast enough even on a personal computer to be used as the method of first recourse for error estimation.

The procedure demonstrated in this report (Fig. 1) is analogous to that employed by Hodges & McKenna (1987) for single thermobarometer pairs, except that we have sampled results of analyses rather than recalculated mineral formulae in order to avoid the problem of compositional closure. One hundred permutations of mineral composition have been sampled from uncorrelated 1% relative (1σ) normal distributions about the nominal weight percent for each oxide in each different solid-solution mineral in each sample. This is a reasonable approximation to the uncertainty resulting from X-ray counting statistics associated with a typical analysis obtained with an electron microprobe: the slight correlations due to matrix-correction procedures have been ignored. From each permutation, a structural formula has been calculated and checked to make sure that all permutations have acceptable totals, charge balance, etc. Sets of these permutations, each forming a complete paragenesis, have been used to calculate 100 separate P-T plots. The resulting P-T intersections, typically ~8000 points for each sample, have then been combined on one diagram and contoured for density, in order to define confidence regions enclosing known proportions of the total population of P-T points. Calculation time using a personal computer is on the order of 1 hour, on faster computers much less. Software for this and other aspects of TWEEQU computation will be made available to the geological community.

GEOLOGICAL SETTINGS

Western Alaska

The samples considered in this report were collected on the southern Seward Peninsula, where rocks of the upper-amphibolite and, locally, granulite facies are exposed in the core of Tertiary antiforms (Fig. 2a). These high-grade units are overlain by rocks of the Jurassic - Cretaceous

Seward Peninsula blueschist terrane, the westernmost portion of an extensive belt of high P-low T metamorphic rocks exposed in the hinterland of the Brooks Range fold-and-thrust belt of northern Alaska (Till *et al.* 1986). The sequence underwent burial to ~12 kbar at ~450°C during the mid-Jurassic (*ca.* 140-160 Ma) (Armstrong *et al.* 1986, Patrick & Evans 1989) followed by a prolonged period (30-50 Ma) of decompression and greenschist-facies overprinting.

On the southern flank of one of these antiforms, the Kigluaik Mountains, a continuous metamorphic gradient from blueschist to granulite facies has been mapped. A Barrovian sequence can be followed on the flank; it reaches its culmination in the core of the range, within lithologies similar to those recognized throughout the blueschist terrane (Till 1980, Till *et al.* 1986). In the biotite and staurolite zones, statically overprinted assemblages and inherited structures indicate that the higher-T minerals overprinted blueschist parageneses (Patrick & Lieberman 1988). In the core of the Kigluaik Mountains, granulite-facies parageneses such as those considered in this report occur in pelitic, quartzofeldspathic, calc-silicate, mafic, and ultramafic gneisses. The granulites are intimately associated with anatectic gneiss and granite (Lieberman 1988, Till 1980).

P-T conditions at the temperature peak have previously been estimated at 800°C and 8 kbar (Lieberman 1988). The timing of the granulite-facies metamorphism has been dated by U-Pb in zircon at 109.5 ± 2.7 Ma (Lieberman & P. van der Heyden, in prep.). The source of heat for the localized attainment of granulite-facies conditions is as yet unclear, but on the basis of oxygen and carbon isotopic studies, is more likely to have been underplating of mafic magmas than infiltration of hot fluids (Todd & Evans 1990). On the basis of the structural continuity between granulite and blueschist, as well as the presence of rare garnet-spinel lherzolites within the granulite zone (Lieberman & Till 1987), some of the mineral assemblages within the granulites may preserve equilibrations to a range of pressures during a prolonged phase of decompression correlated to that of the blueschists.

Moldanubia

The two samples considered in this report belong to the Moldanubian zone of the Austrian part of the Bohemian Crystalline Complex. Although the internal structure and the nature of the Moldanubian zone are still matters of controversy among Austrian geologists (Fuchs 1976, Fuchs & Matura 1976, 1980, Matura 1976, Thiele 1976, 1984,

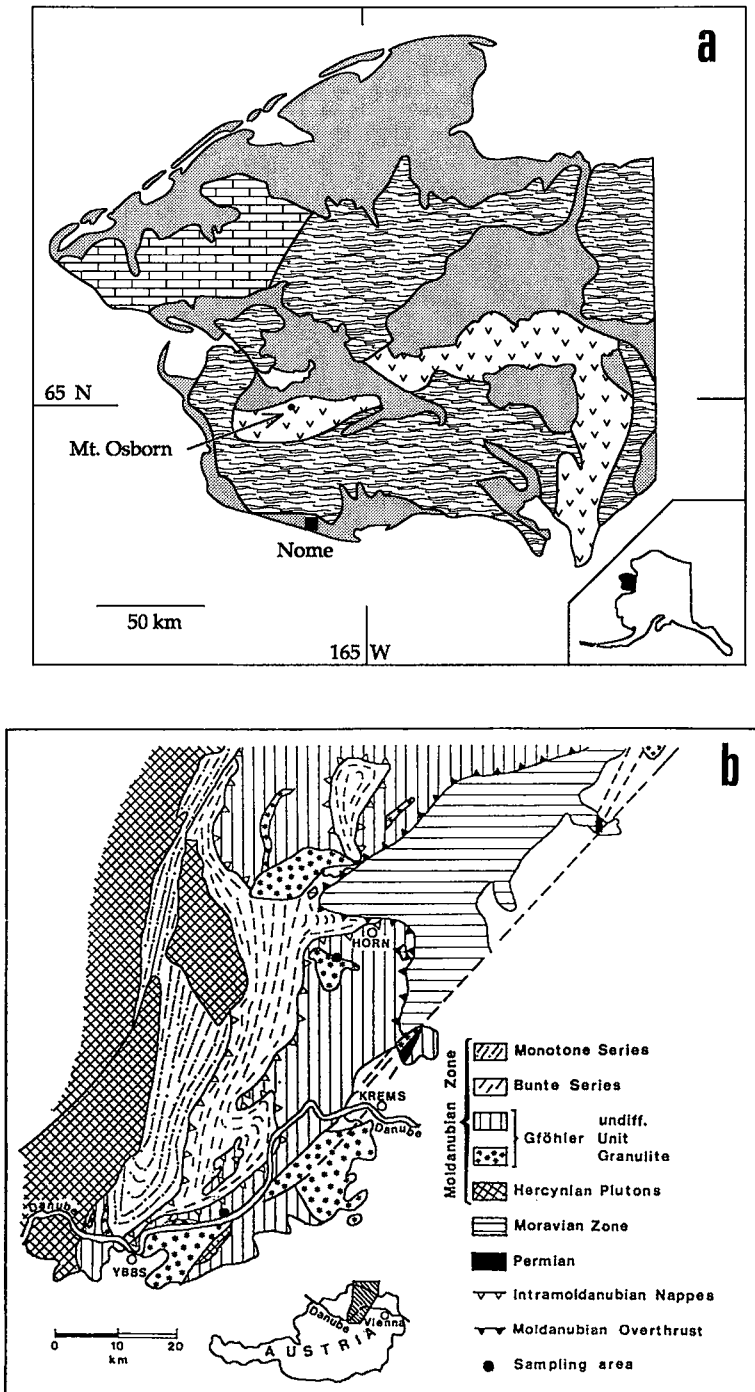


FIG. 2. a. Location map of Kigluaiik granulites. Quaternary cover in grey, York Mountains sediments in a box pattern, blueschists and marbles in a wavy pattern, and high-grade schists, gneisses, and marbles of the Kigluaiik, Bendeleben, and Darby Mountains in a V pattern. Granulite-facies rocks occur at the base of the Kigluaiik Mountains section; the two samples used in this study were collected from the west flank of Mt. Osborn. b. Location map of Gföhl gneiss. Units as shown. The locations of the two samples used in this study are indicated with dots.

Tollmann 1982, 1985), we summarize in this report the regional picture as given by Fuchs. The Moldanubian zone is composed of three units generally striking NNE-SSW and dipping east (Fig. 2b). All of them may be followed farther north into Czechoslovakia. To the south, they disappear under Alpine molasse sediments. The eastern boundary of the Moldanubian zone is formed by a tectonic contact against the underlying Moravian zone. To the west, the Moldanubian rocks are cut off by Hercynian granitic rocks of the Southern Bohemian Pluton. Recent U-Pb studies of Bohemian granulites in Czechoslovakia (Kröner *et al.* 1988, Van Breemen *et al.* 1982) show lower intercept ages (367–347 Ma), which most likely resulted from Hercynian metamorphism of Proterozoic to Archean sediments.

The lowest unit, the Monotone Series, is composed of a sequence of (Crd + Bt + Kfs + Sil + Ms)-bearing gneisses, (Bt + Sil + Ms)-bearing gneisses and leucocratic (Sil + Kfs + Bt ± Ms)-bearing gneisses, with occasional calc-silicate boudins (Linner 1990, pers. comm.). A thin horizon of platy, highly deformed blastomylonite, or "granulite lamella" (Fuchs & Scharbert 1979, Petrakakis 1986) separates the Monotone Series from the overlying Bunte Series. The latter is composed of various types of metapelites (Gr + Bt + Sil + Kfs), quartzofeldspathic rocks, amphibolite, graphitic schist, calc-silicate rocks, and marble.

The Gföhl unit represents the highest part of the Moldanubian zone. The contact that separates the marble-rich top of the Bunte Series from the amphibolite sequences at the base of the Gföhl unit (Fuchs 1976, Fuchs & Matura 1976, Matura 1976) lacks a clearly tectonic character. The Gföhl unit is composed of the migmatitic Gföhl gneiss, syenite gneiss, meta-anorthosite, (Gr + Cpx)-bearing amphibolites, Cpx gneisses, (Opx + Bt)-bearing gneisses and (± Opx) granulites. The latter occur at the highest tectonic position within the Gföhl unit. A very typical feature of this unit is the occurrence of (now serpentized) mantle-derived ultramafic rocks with associated metabasalts (Carswell *et al.* 1989, Scharbert & Carswell 1983). The most widespread rocks of this unit, the Gföhl gneiss and the pyroxene-free granulites, show the same characteristic mineral assemblage (*i.e.*, Gr + Bt + Sil + Kfs), but differ in their degree of deformation (Petrakakis & Richter 1990).

Fuchs (1976) postulated a bottom-to-top increase in the grade of metamorphism from west to east within the Moldanubian zone, culminating in the granulites of the Gföhl unit. Reliable determinations of the grade of metamorphism in the lowermost Monotone Series have been lacking to

date. The conditions of metamorphism of the Bunte Series are estimated at 700–770°C and 7–9 kbar (Högelsberger 1989, and references therein, Petrakakis 1986). Older estimates of the metamorphic grade of the Gföhl granulites (Scharbert & Kurat 1974) are 760°C and 11 kbar. This raises the question as to whether the P-T conditions of metamorphism for both units are significantly different. If not, a tectonic contact between the two units, at the base of the Gföhl gneiss-and-granulite complex, might have predated the main metamorphism of Hercynian age (W. Frank, 1990 pers. comm.).

PETROGRAPHIC RELATIONS AND MINERAL CHEMISTRY

Analytical methods

Analyses of the Alaskan samples were performed on a JEOL 733 Superprobe (University of Washington). Operating conditions were 15 kV, 35 nA, with counting times sufficient for at least ± 1% (1σ) precision in major elements. Both synthetic and natural standards were used, and the matrix correction followed the method of Bence & Albee (1968). Mineral formulae were calculated by electronic spreadsheet. Analyses of Moldanubian samples were carried out on an ARL-SEM microprobe (University of Bern), operated at 15 kV and 20 nA. Both natural and synthetic standards, and a ZAF matrix correction were used. Mineral formulae were calculated with the program MIN-SORT (Petrakakis & Dietrich 1985). Where reported values are averages of more than two individual analyses, the standard deviation for each oxide also is reported (Tables 2–7). Full variance-covariance matrices are available upon request. Mineral abbreviations throughout this report follow the recommendations of Kretz (1983).

Kigluaik Mountains

Sample AB86-110.3 ("86-110.3"), a mafic, slightly banded two-pyroxene granulite, was collected from near the base of the Kigluaik section in the west cirque of Mt. Osborn. It contains the assemblage grt + cpx + opx + pl + Qtz + hbl + bt + ilm + rt + gr ± ap ± zrn (Fig. 3a). Amphibole is abundant, and biotite, rarer. Banding is defined by amphibole-rich and pyroxene-rich layers, but mineral textures are largely granoblastic. Exceptions are a very weak foliation defined by biotite, and symplectite textures of hbl + opx + Qtz + pl around many garnet porphyroblasts. The common occurrence of such symplectite without garnet in amphibole-rich layers indicates the former

TABLE 2. ELECTRON-MICROPROBE DATA ON ILMENITE

Sample Position	GE31		SL40	
	matrix Statistic	incl in opx $\mu_2 \pm 1\sigma$	matrix μ_2	incl in gar $\mu_4 \pm 1\sigma$
SiO ₂	0.05±0.05	0.00	0.08	0.04±0.03
TiO ₂	50.39±0.80	49.95	48.85	49.91±0.49
Al ₂ O ₃	0.00	0.00	0.00	0.00
Cr ₂ O ₃	0.00	0.00	0.11	0.10±0.03
FeO	49.74±0.45	51.13	48.85	48.81±0.32
MnO	0.75±0.14	0.85	2.12	1.35±0.18
MgO	0.12±0.14	0.49	0.00	0.25±0.15
CaO	0.00	0.00	0.36	0.16±0.09
Total	101.05±0.67	102.41	100.35	100.63±0.44
Si	0.001	0.000	0.002	0.001
Al	0.000	0.000	0.000	0.000
Ti	0.943	0.919	0.919	0.936
Cr	0.000	0.000	0.002	0.002
Fe ³⁺	0.056	0.081	0.078	0.062
Fe ²⁺	0.924	0.883	0.867	0.895
Mg	0.005	0.018	0.000	0.009
Mn	0.016	0.018	0.045	0.029
Ca	0.000	0.000	0.010	0.004
ilm	0.924	0.883	0.876	0.900
gei	0.005	0.018	0.000	0.010
prph	0.016	0.018	0.045	0.029
hem	0.056	0.081	0.079	0.062

Formula to 2 cations, 3 oxygen atoms

presence of more garnet grains than presently observed. Grain sizes are small to medium (except for garnet grains up to 1 mm in diameter). Matrix ilmenite is more abundant than rutile; among garnet inclusions, the proportion is reversed. Granoblastic plagioclase grains commonly show striking optical zoning, but plagioclase grains in

symplectite regions around garnet appear unzoned. Textures are generally clean, with little evidence of lower-temperature alteration.

Chemically, the garnet grains are only slightly zoned, with a rim enriched in Fe, Mn, and Ca (likely the result of some resorption). Plagioclase compositions are variable, but zoned grains range on average from An₆₉ in the core to An₈₉ in the rim. Orthopyroxene is relatively uniform in composition, even including symplectite grains, except for a small core-rim decrease in Al. The clinopyroxene is more significantly zoned, with (Al + Fe³⁺ + Na)-enriched rims, but Fe-Mg zoning is again minor.

Sample AB86-117.4 ("86-117.4"), a slightly banded, light gray gneiss from the same locality as AB86-110.3, has the assemblage grt + cpx + opx + pl + qtz + bt + ilm ± ap ± zrn (Fig. 3b), with much more abundant biotite than in the previous sample. Banding is defined by variations in abundance of weakly foliated biotite and stringers of granoblastic cpx + opx + gar in a matrix of slightly deformed granoblastic pl + qtz. The pyroxene and biotite foliations are not always parallel, providing weak evidence that the biotite recrystallized at a later time than the pyroxene. Grain sizes are not greatly variable, and average 1 mm in diameter. Garnet forms rounded or slightly embayed porphyroblasts, with rare patchy development of opx + pl as a symplectitic rim. Matrix plagioclase may have weak optical zoning. Quartz grains are small, equant, and unstrained. Minerals are generally clean and unaltered, except for rare sericitization of plagioclase and rare patches of

TABLE 3. ELECTRON-MICROPROBE DATA ON GARNET

Sample: Position	GE31		SL40		86-110.3		86-117.4	
	rim Statistic	core $\mu_{15} \pm 1\sigma$	rim $\mu_{20} \pm 1\sigma$	core $\mu_{14} \pm 1\sigma$	core $\mu_7 \pm 1\sigma$	rim $\mu_5 \pm 1\sigma$	core $\mu_4 \pm 1\sigma$	rim $\mu_4 \pm 1\sigma$
SiO ₂	38.66±0.22	38.79±0.14	38.75±0.33	38.74±0.40	38.93±0.16	39.26±0.27	37.99±0.23	38.49±0.40
TiO ₂	0.03±0.08	0.06±0.08	0.05±0.04	0.07±0.03	0.08±0.20	0.02±0.01	0.10±0.04	0.08±0.03
Al ₂ O ₃	21.87±0.32	21.98±0.16	21.63±0.22	21.56±0.20	22.19±0.20	22.31±0.13	20.77±0.13	20.87±0.41
Cr ₂ O ₃	0.00	0.00	0.06±0.05	0.04±0.04	N/A	N/A	N/A	N/A
FeO	27.83±0.99	24.13±0.29	25.31±0.85	24.44±0.67	22.78±0.42	23.30±0.20	28.38±0.33	26.67±0.62
MnO	2.39±0.22	2.13±0.18	1.37±0.14	1.14±0.07	0.83±0.09	0.97±0.10	2.13±0.52	2.49±0.51
MgO	5.75±0.58	5.66±0.50	5.79±0.44	6.80±0.33	9.72±0.47	9.37±0.43	3.70±0.28	3.06±0.29
CaO	4.99±0.84	8.39±0.28	8.16±0.43	8.01±0.56	5.18±0.28	5.51±0.14	7.34±0.34	7.25±0.42
Total	101.54±0.59	101.14±0.33	101.12±0.45	100.81±0.67	99.72±0.50	100.73±0.53	100.40±0.33	98.31±1.10
Si	2.984	2.981	2.982	2.973	2.971	2.974	3.005	3.095
[4]Al	0.016	0.019	0.020	0.028	0.029	0.026	0.000	0.000
[6]Al	1.974	1.972	1.942	1.922	1.968	1.967	1.947	2.169
Cr	0.000	0.000	0.004	0.003	-	-	-	-
Ti	0.003	0.003	0.003	0.004	0.005	0.001	0.006	0.005
Fe ³⁺	0.027	0.030	0.056	0.077	0.051	0.056	0.041	0.000
Fe ²⁺	1.770	1.521	1.573	1.492	1.403	1.420	1.837	1.792
Mn	0.156	0.139	0.089	0.074	0.044	0.051	0.117	0.139
Mg	0.662	0.649	0.665	0.778	1.105	1.057	0.436	0.366
Ca	0.413	0.691	0.673	0.658	0.424	0.447	0.622	0.625
alm	0.390	0.507	0.525	0.497	0.458	0.464	0.595	0.636
sps	0.052	0.046	0.030	0.025	0.015	0.017	0.038	0.045
prp	0.221	0.216	0.222	0.259	0.361	0.345	0.142	0.118
gns	0.123	0.214	0.193	0.178	0.138	0.146	0.202	0.202
"adr"	0.015	0.017	0.029	0.040	0.028	0.028	0.024	0.000

Formula to 8 cations and 12 oxygen atoms, "and" = (Fe³⁺+Ti)/(6[Al]+Fe³⁺+Ti)

TABLE 3 (CONTINUED). ELECTRON-MICROPROBE DATA ON GARNET

Sample Number	SL40 selected	Pt. 128	Pt. 159	Pt. 165	Pt. 180	Pt. 181	Pt. 196	Pt. 203	Pt. 204	Pt. 208	Pt. 204	Pt. 208
SiO ₂	38.66	38.95	38.95	39.15	39.52	39.16	38.83	38.71	39.15	38.71	39.15	39.15
TiO ₂	0.08	0.21	0.08	0.05	0.04	0.09	0.11	0.12	0.05	0.12	0.05	0.05
Al ₂ O ₃	21.84	21.95	22.08	21.21	21.44	21.45	21.08	21.04	21.27	21.04	21.27	21.27
Cr ₂ O ₃	0.00	0.00	0.00	0.00	0.00	0.00	0.00	0.00	0.06	0.00	0.00	0.06
FeO	23.94	24.39	25.34	24.52	23.91	24.60	24.86	24.73	24.79	24.73	24.79	24.79
MnO	1.10	1.02	1.13	0.98	1.05	1.01	1.13	1.06	1.08	1.06	1.08	1.08
MgO	6.65	7.50	6.59	7.10	6.98	6.73	6.23	6.68	6.66	6.68	6.66	6.66
CaO	8.36	7.81	7.56	7.52	7.75	7.92	7.82	7.74	7.60	7.74	7.60	7.60
Total	100.63	101.83	101.73	100.53	100.69	100.96	100.06	100.08	100.66	100.08	100.66	100.66
Si	2.969	2.951	2.968	3.005	3.021	2.999	3.007	2.994	3.008	2.994	3.008	3.008
[⁴ Al]	0.031	0.049	0.032	0.000	0.000	0.001	0.000	0.006	0.000	0.006	0.000	0.000
[⁶ Al]	1.946	1.911	1.952	1.919	1.931	1.934	1.924	1.912	1.926	1.912	1.926	1.926
Cr	0.000	0.000	0.000	0.000	0.000	0.000	0.000	0.000	0.004	0.000	0.004	0.004
Ti	0.005	0.012	0.005	0.003	0.002	0.005	0.006	0.007	0.003	0.007	0.003	0.003
Fe ³⁺	0.055	0.086	0.050	0.077	0.061	0.059	0.067	0.081	0.065	0.081	0.065	0.065
Fe ²⁺	1.483	1.459	1.565	1.497	1.467	1.516	1.543	1.519	1.527	1.519	1.527	1.527
Mn	0.072	0.065	0.073	0.064	0.068	0.066	0.074	0.069	0.070	0.069	0.070	0.070
Mg	0.761	0.847	0.749	0.812	0.795	0.768	0.719	0.770	0.763	0.770	0.763	0.763
Ca	0.688	0.634	0.617	0.618	0.635	0.630	0.649	0.641	0.626	0.641	0.626	0.626
alm	0.494	0.485	0.521	0.500	0.495	0.505	0.517	0.506	0.511	0.506	0.511	0.511
sps	0.024	0.022	0.024	0.021	0.023	0.022	0.025	0.023	0.024	0.023	0.024	0.024
pyr	0.254	0.282	0.249	0.272	0.268	0.256	0.241	0.257	0.255	0.257	0.255	0.255
grs	0.199	0.162	0.178	0.167	0.182	0.184	0.180	0.170	0.173	0.170	0.173	0.173
"adr"	0.030	0.049	0.027	0.040	0.032	0.032	0.037	0.044	0.034	0.044	0.034	0.034

Formula to 8 cations and 12 oxygen atoms; "adr" = $(\text{Fe}^{3+} + \text{Ti}) / ([⁶]\text{Al} + \text{Fe}^{3+} + \text{Ti})$.

uralitic amphibole around pyroxene. Ilmenite, zircon, and apatite are common accessory minerals, but no rutile occurs.

Most minerals are characterized by relatively uniform compositions. Garnet rims have slightly higher Fe/Mg ratios, and more variable analytical totals than cores. Plagioclase is weakly zoned from An₄₁ to An₄₆. Biotite rims are lower in Ti and K than cores, possibly reflecting incipient chloritization.

Moldanubia

Sample 88-GE-31 ("GE31") is a mafic, slightly banded gneiss bearing the assemblage grt + opx + bt + pl + qtz + ilm + rt ± ap ± py ± zrn (Fig. 4a); it is associated with grt-cpx amphibolites exposed in the railway station yard of Weitenegg village. Gneissic banding is defined by alternating (bt + grt + opx)-rich and (pl + qtz)-rich layers, whereas under the microscope a foliation is defined

TABLE 4. ELECTRON-MICROPROBE DATA ON PYROXENE

Sample:	GE31	opx	86-110.3	opx	86-110.3	cpx	86-117.4	opx	86-117.4	cpx	
Position:	core	rim	core	rim	core	rim	small	core	rim	core	
Statistic	$\mu_{10} \pm 1\sigma$	$\mu_{10} \pm 1\sigma$	μ_2	μ_2	μ_2	μ_2	1	$\mu_3 \pm 1\sigma$	$\mu_3 \pm 1\sigma$	$\mu_3 \pm 1\sigma$	
SiO ₂	51.00±0.47	50.77±0.50	52.79	52.86	52.35	50.76	51.95	49.98±0.26	50.04±0.15	50.83±0.11	51.15±0.47
TiO ₂	0.09±0.04	0.09±0.05	0.13	0.14	0.38	0.62	0.22	0.09±0.01	0.08±0.01	0.28±0.14	0.13±0.01
Al ₂ O ₃	1.63±0.10	1.79±0.10	1.70	1.46	2.09	3.70	1.18	0.56±0.07	0.51±0.10	1.87±0.58	1.17±0.05
Cr ₂ O ₃	0.00	0.00	N/A	N/A	N/A	N/A	N/A	N/A	N/A	N/A	N/A
FeO	26.87±0.24	26.82±0.61	22.25	21.98	7.38	8.03	7.79	33.72±0.29	33.74±0.20	14.59±0.51	14.50±0.36
MnO	0.70±0.05	0.72±0.10	0.51	0.49	0.19	0.18	0.20	0.96±0.07	0.96±0.06	0.38±0.01	0.39±0.04
MgO	19.64±0.88	20.23±1.12	22.93	23.07	14.78	14.77	15.11	14.02±0.05	14.27±0.04	11.01±0.37	11.05±0.01
CaO	0.27±0.23	0.04±0.14	0.59	0.60	23.03	20.59	22.77	0.92±0.05	0.92±0.05	20.58±0.73	21.32±0.22
Na ₂ O	0.00	0.00	0.02	0.03	0.22	0.64	0.19	0.00±0.0	0.00±0.0	0.28±0.07	0.20±0.04
K ₂ O	0.00	0.00	N/A	N/A	N/A	N/A	N/A	N/A	N/A	N/A	N/A
Total	100.22±0.73	100.47±0.78	100.94	100.69	100.47	99.33	99.42	100.31±0.49	100.54±0.37	99.85±0.09	99.97±0.76
Si	1.931	1.913	1.942	1.948	1.929	1.884	1.934	1.970	1.965	1.941	1.954
[⁴ Al]	0.068	0.080	0.058	0.052	0.071	0.116	0.066	0.030	0.035	0.059	0.046
[⁶ Al]	0.005	0.000	0.016	0.011	0.019	0.046	-0.014	-0.004	-0.011	0.026	0.006
Ti	0.003	0.002	0.004	0.004	0.011	0.017	0.006	0.003	0.002	0.008	0.004
Cr	0.000	0.000	-	-	-	-	-	-	-	-	-
Fe ³⁺	0.059	0.088	0.035	0.034	0.045	0.081	0.082	0.029	0.041	0.037	0.047
Fe ²⁺	0.792	0.750	0.650	0.643	0.182	0.168	0.161	1.082	1.067	0.429	0.414
Mn	0.023	0.023	0.013	0.012	0.005	0.005	0.005	0.026	0.026	0.010	0.010
Mg	1.108	1.136	1.257	1.267	0.812	0.817	0.838	0.824	0.835	0.626	0.629
Ca	0.011	0.002	0.023	0.023	0.909	0.819	0.908	0.039	0.039	0.842	0.873
Na	0.000	0.000	0.001	0.002	0.016	0.046	0.014	0.000	0.000	0.021	0.015
K	0.000	0.000	-	-	-	-	-	-	-	-	-
X _{Mg}	0.584	0.603	0.659	0.663	0.817	0.829	0.839	0.432	0.439	0.593	0.602

Formula to 4 cations and 6 oxygen atoms

TABLE 4 (CONTINUED). ELECTRON-MICROPROBE DATA ON PYROXENE

Sample:	SL40	cpx	selected						
Position	core	rim							
Statistic	$\mu_{20} \pm 1\sigma$	$\mu_{16} \pm 1\sigma$	Pt. 158	Pt. 167	Pt. 177	Pt. 178	Pt. 179	Pt. 201	Pt. 205
SiO ₂	50.66±0.86	51.51±0.60	51.56	50.15	51.78	51.15	51.14	51.00	50.87
TiO ₂	0.64±0.07	0.43±0.09	0.40	0.58	0.39	0.38	0.37	0.58	0.59
Al ₂ O ₃	4.71±0.64	3.27±0.66	3.68	4.07	2.65	3.84	3.15	3.48	3.73
Cr ₂ O ₃	0.05±0.04	0.03±0.04	0.00	0.00	0.00	0.00	0.00	0.06	0.00
FeO	9.80±0.32	9.67±0.23	8.55	9.01	8.70	9.07	8.62	8.07	8.53
MnO	0.24±0.02	0.23±0.04	0.13	0.19	0.21	0.15	0.16	0.13	0.12
MgO	12.30±0.29	12.61±0.48	13.04	12.52	13.19	12.84	12.99	12.95	12.72
CaO	22.13±0.67	22.43±0.68	22.04	22.12	22.46	22.44	22.35	22.67	22.46
Na ₂ O	0.66±0.08	0.52±0.06	0.55	0.58	0.54	0.52	0.49	0.56	0.57
K ₂ O	0.01±0.01	0.00±0.01	0.00	0.00	0.00	0.00	0.04	0.00	0.00
Total	101.20±1.05	100.72±1.05	99.95	99.22	99.92	100.39	99.31	99.50	99.59
Si	1.868	1.911	1.917	1.882	1.928	1.897	1.916	1.904	1.900
[4]Al	0.132	0.089	0.083	0.118	0.072	0.103	0.084	0.096	0.100
[6]Al	0.073	0.054	0.078	0.062	0.044	0.065	0.055	0.057	0.065
Ti	0.018	0.012	0.011	0.016	0.011	0.011	0.010	0.016	0.017
Cr	0.002	0.001	0.000	0.000	0.000	0.000	0.000	0.002	0.000
Fe ³⁺	0.069	0.052	0.022	0.065	0.045	0.055	0.046	0.044	0.043
Fe ²⁺	0.233	0.248	0.244	0.218	0.224	0.226	0.223	0.207	0.223
Mn	0.007	0.007	0.004	0.006	0.007	0.005	0.005	0.004	0.004
Mg	0.676	0.697	0.723	0.701	0.732	0.710	0.725	0.721	0.708
Ca	0.875	0.891	0.878	0.890	0.896	0.892	0.897	0.907	0.899
Na	0.047	0.037	0.040	0.042	0.039	0.037	0.036	0.041	0.041
K	0.000	0.000	0.000	0.000	0.000	0.000	0.002	0.000	0.000
X _{Mg}	0.744	0.738	0.748	0.763	0.764	0.758	0.764	0.776	0.760

Formula to 4 cations and 6 oxygen atoms

by biotite. Grain size is variable, up to 3 mm, with some shape-preferred orientation of quartz. Both quartz and plagioclase show undulatory extinction. Textures are slightly deformed granoblastic, with well-preserved triple junctions. Except for rare traces of uraltic brown hornblende at opx-pl junctions, secondary minerals are absent.

Garnet grains are typically less than 0.4 mm in diameter, idioblastic to hypidioblastic. Rarer 1.0–1.5 mm diameter grains have inclusions of ilmenite and rutile, show slightly resorbed rims, and are

usually surrounded by biotite. Some smaller garnet grains are themselves included in larger opx grains. Figure 5a shows three representative compositional profiles of garnet. The Mn profile for the largest grain suggests that some original growth-zoning (zone A) may not have been erased entirely within the core, but that the rim compositions (zone B) are the result of resorption and retrograde re-equilibration. Profiles for the two smaller grains are dominated (except in the cores) by retrograde re-equilibration and diffusion. Orthopyroxene is

TABLE 5. ELECTRON-MICROPROBE DATA ON PLAGIOCLASE

Sample:	GE31	SL40			"relict"		86-110.3		86-117.4			
Position	rim	core	profile	rim	low-Ca core	rim in gar	core	core	rim	small	core	rim
Statistic	$\mu_9 \pm 1\sigma$	$\mu_4 \pm 1\sigma$	$\mu_{20} \pm 1\sigma$	$\mu_6 \pm 1\sigma$	$\mu_3 \pm 1\sigma$	$\mu_3 \pm 1\sigma$	1	$\mu_3 \pm 1\sigma$	μ_2	1	$\mu_3 \pm 1\sigma$	$\mu_6 \pm 1\sigma$
SiO ₂	56.47±0.87	58.27±0.22	54.80±0.61	54.95±0.82	55.03±0.69	54.66±0.76	63.30	51.61±5.32	46.20	44.84	58.10±0.29	57.18±0.57
TiO ₂	0.00	0.04±0.07	0.00	0.00	0.00	0.00	0.00	N/A	N/A	N/A	N/A	N/A
Al ₂ O ₃	26.75±0.49	26.03±0.49	28.34±0.58	28.73±0.55	27.87±0.39	28.90±1.32	22.34	31.36±3.39	34.60	34.95	26.51±0.21	27.30±0.25
FeO	0.27±0.31	0.11±0.04	0.07±0.03	0.09±0.02	0.04±0.03	0.32±0.07	0.00	0.08±0.01	0.11	0.58	0.19±0.15	0.25±0.12
MgO	0.26±0.69	0.13±0.26	0.00	0.00	0.00	0.00	0.00	N/A	N/A	N/A	N/A	N/A
CaO	9.21±0.57	7.57±0.20	10.58±0.41	10.85±0.39	10.01±0.31	11.26±0.40	3.06	14.09±3.79	17.57	18.17	8.67±0.12	9.52±0.40
Na ₂ O	5.79±0.28	6.53±0.34	5.77±0.24	5.68±0.38	6.00±0.12	5.24±0.18	10.23	3.54±2.38	1.21	0.57	6.32±0.27	6.00±0.18
K ₂ O	0.70±0.09	0.78±0.07	0.06±0.02	0.05±0.02	0.06±0.02	0.21±0.29	0.09	0.05±0.05	0.00	0.00	0.75±0.41	0.46±0.22
Total	99.45±0.90	99.46±0.65	99.61±0.86	100.35±0.90	99.01±1.14	100.59±0.78	99.02	100.73±0.55	99.68	99.11	100.55±0.34	100.72±0.18
Si	2.556	2.621	2.481	2.471	2.502	2.457	2.824	2.329	2.134	2.093	2.594	2.553
Al	1.427	1.380	1.512	1.522	1.494	1.531	1.174	1.673	1.884	1.924	1.395	1.436
Ti	0.000	0.001	0.000	0.000	0.000	0.000	0.000	-	-	-	-	-
Fe	0.010	0.004	0.003	0.004	0.001	0.012	0.000	0.003	0.004	0.023	0.007	0.009
Mg	0.018	0.009	0.000	0.000	0.000	0.000	0.000	-	-	-	-	-
Ca	0.447	0.365	0.513	0.523	0.488	0.542	0.146	0.684	0.870	0.909	0.415	0.455
Na	0.508	0.570	0.506	0.495	0.529	0.456	0.885	0.308	0.108	0.052	0.547	0.520
K	0.040	0.045	0.003	0.003	0.004	0.012	0.005	0.003	0.000	0.000	0.043	0.026
an	0.449	0.373	0.502	0.512	0.478	0.537	0.141	0.687	0.890	0.946	0.413	0.455
ab	0.511	0.582	0.495	0.485	0.518	0.452	0.854	0.310	0.110	0.054	0.544	0.519
or	0.041	0.046	0.003	0.003	0.004	0.012	0.005	0.003	0.000	0.000	0.043	0.026

Formula to 5 cations

TABLE 6. ELECTRON-MICROPROBE DATA ON BIOTITE

Sample:	GE31			86-110.3		86-117.4		
Position	matrix core	rim to gar	incl in gar	core	core	rim	small	
Statistic	$\mu_8 \pm 1\sigma$	$\mu_{10} \pm 1\sigma$	μ_2	$\mu_4 \pm 1\sigma$	$\mu_4 \pm 1\sigma$	$\mu_4 \pm 1\sigma$	μ_2	
SiO ₂	35.76±0.30	36.04±0.32	36.68	37.91±0.35	35.64±0.06	36.79±1.86	35.50	
TiO ₂	4.50±0.24	4.36±0.22	4.75	3.29±0.33	5.94±0.26	5.54±0.51	5.45	
Al ₂ O ₃	15.85±0.32	15.85±0.41	16.16	15.32±0.31	14.08±0.07	14.15±0.29	14.05	
Cr ₂ O ₃	0.00	0.00	0.00	N/A	N/A	N/A	N/A	
FeO	17.43±0.26	17.07±0.74	15.47	10.37±0.18	22.01±0.25	20.82±1.74	22.08	
MnO	0.06±0.03	0.06±0.04	0.09	0.03±0.01	0.12±0.01	0.10±0.02	0.11	
MgO	12.64±0.28	12.89±0.49	13.59	18.29±0.12	9.42±0.19	9.00±0.81	9.53	
CaO	0.00	0.00	0.00	0.00	0.01±0.01	0.41±0.63	0.03	
Na ₂ O	0.16±0.04	0.23±0.09	0.22	0.70±0.12	0.06±0.02	0.06±0.21	0.02	
K ₂ O	9.39±0.29	9.36±0.25	9.23	9.35±0.18	9.55±0.18	8.98±0.81	9.35	
F	N/A	N/A	N/A	N/A	0.88±0.05	0.86±0.06	0.92	
H ₂ O calc	N/A	N/A	N/A	4.10±0.03	3.08±0.06	3.12±0.09	3.02	
Total	95.79±0.53	95.86±0.49	96.19	99.36±0.75	100.76±0.32	99.90±0.73	100.03	
Si	2.644	2.661	2.671	2.772	2.727	2.807	2.735	
Ti	0.250	0.242	0.260	0.181	0.342	0.318	0.315	
[4]Al	1.356	1.339	1.329	1.228	1.273	1.193	1.265	
[6]Al	0.025	0.040	0.057	0.092	0.000	0.079	0.011	
Cr	0.000	0.000	0.000	-	-	-	-	
Fe	1.078	1.054	0.942	0.634	1.408	1.330	1.422	
Mn	0.004	0.004	0.006	0.002	0.006	0.005	0.006	
Mg	1.393	1.419	1.475	1.993	1.074	1.024	1.094	
Ca	0.000	0.000	0.000	0.000	0.001	0.033	0.002	
Na	0.023	0.033	0.031	0.099	0.009	0.024	0.002	
K	0.886	0.881	0.857	0.872	0.932	0.875	0.919	
F	N/A	N/A	N/A	N/A	0.213	0.206	0.223	
X _{Mg}	0.564	0.574	0.610	0.759	0.433	0.435	0.435	

Formula to 11 oxygen atoms + water

TABLE 7. ELECTRON-MICROPROBE DATA ON AMPHIBOLE

Sample:	SL40								86-110.3			
Position	matrix core	rim	incl in cpx	selected	Pt. 197	Pt. 198	Pt. 226	Pt. 227	Pt. 231	Pt. 247	core	rim
Statistic	$\mu_{21} \pm 1\sigma$	$\mu_7 \pm 1\sigma$	$\mu_3 \pm 1\sigma$								$\mu_4 \pm 1\sigma$	μ_2
SiO ₂	42.51±0.57	42.69±0.53	42.52±0.31	43.00	42.98	43.67	43.31	44.02	45.72	43.62±0.82	44.26	
TiO ₂	1.92±0.15	1.79±0.13	2.07±0.13	1.73	1.72	1.59	1.71	1.75	1.36	1.72±0.21	1.65	
Al ₂ O ₃	12.59±0.50	12.28±0.52	12.15±0.41	12.96	13.05	11.99	11.95	11.96	11.54	12.70±0.47	12.05	
Cr ₂ O ₃	0.09±0.03	0.09±0.02	0.09±0.01	0.07	0.07	0.13	0.13	0.10	0.18	N/A	N/A	
FeO	14.77±0.30	14.62±0.35	14.60±0.23	12.22	12.06	12.89	13.47	13.21	11.04	11.03±0.42	11.14	
MnO	0.15±0.02	0.15±0.02	0.16±0.06	0.10	0.13	0.11	0.08	0.12	0.10	0.08±0.10	0.00	
MgO	11.48±0.36	11.63±0.32	11.20±0.09	13.00	12.95	12.98	12.68	12.69	14.49	14.35±0.10	14.73	
CaO	11.71±0.26	11.73±0.38	11.45±0.05	11.80	11.53	12.16	12.05	12.00	11.85	10.70±0.41	11.30	
Na ₂ O	2.15±0.11	2.07±0.11	2.10±0.09	2.21	2.03	1.74	1.98	1.83	1.67	2.45±0.58	2.14	
K ₂ O	0.30±0.03	0.29±0.03	0.30±0.03	0.25	0.29	0.30	0.27	0.29	0.08	0.00	0.07	
H ₂ O calc	-	-	-	-	-	-	-	-	-	2.05±0.02	2.06	
Total	97.68±1.04	97.33±1.16	96.63±1.18	97.34	96.81	97.56	97.63	97.97	98.03	98.97±0.81	99.38	
Si	6.247	6.287	6.317	6.259	6.263	6.356	6.325	6.388	6.502	6.391	6.452	
[4]Al	1.753	1.713	1.683	1.741	1.737	1.644	1.675	1.612	1.498	1.609	1.548	
[6]Al	0.428	0.417	0.444	0.482	0.504	0.412	0.382	0.434	0.437	0.585	0.522	
Ti	0.213	0.198	0.231	0.189	0.188	0.174	0.188	0.191	0.145	0.190	0.180	
Cr	0.010	0.011	0.010	0.008	0.008	0.015	0.015	0.011	0.020	-	-	
Fe ³⁺	0.533	0.543	0.459	0.522	0.620	0.530	0.521	0.484	0.663	-	-	
Mn	0.018	0.019	0.020	0.012	0.016	0.014	0.010	0.015	0.012	0.009	0.000	
Mg	2.516	2.554	2.480	2.821	2.813	2.816	2.761	2.745	3.072	3.133	3.200	
Fe ²⁺	1.282	1.259	1.356	0.965	0.850	1.039	1.124	1.120	0.650	1.352	1.358	
Ca	1.844	1.851	1.823	1.840	1.800	1.896	1.885	1.866	1.806	1.680	1.765	
Na	0.613	0.590	0.605	0.624	0.574	0.491	0.561	0.515	0.460	0.695	0.603	
K	0.056	0.054	0.057	0.046	0.054	0.056	0.050	0.054	0.015	0.044	0.012	
X _{Mg}	0.663	0.670	0.647	0.745	0.768	0.731	0.711	0.710	0.825	0.699	0.702	

SL40: Formula to 13 cations -(CaNaK) and 23 oxygen atoms + water. 86-110.3: Formula to 23 oxygen atoms + water

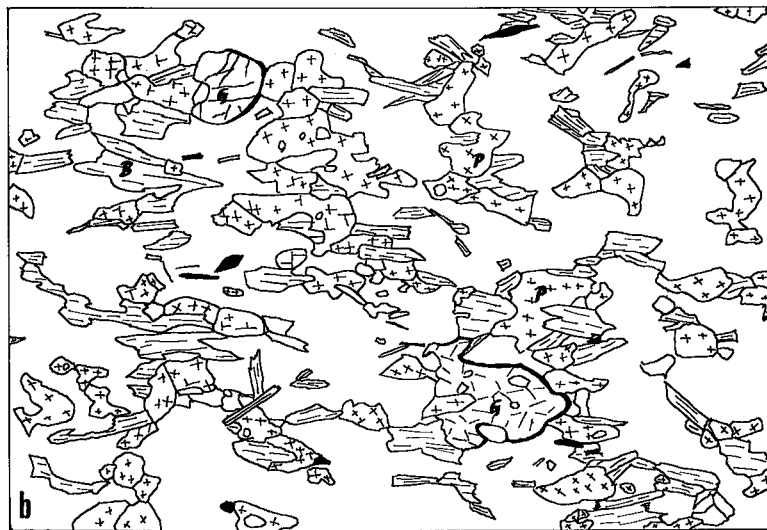


FIG. 3. Mineral textures in thin section. a. Drawing of observed microscopic textures in Kigluaik sample 86-110.3: Symbols: + pyroxenes, x amphibole, - - biotite, (shaded) garnet; white: plagioclase and quartz, black: ilmenite or graphite. Symplectite minerals include both amphibole *and* pyroxene. Rutile, apatite, and zircon not shown. b. Textures in sample 86-117.4: mineral symbols as above. Field of view in both drawings ~5 mm.

granoblastic, unzoned, and evenly distributed, with grain sizes up to 1.5 mm. Inclusions of ilmenite, rutile and (rarely) garnet are found. Plagioclase is xenoblastic, twinned, and inversely zoned from

An₄₇ to An₃₆. Ilmenite is a common accessory mineral both in the matrix of the rock and as inclusions within garnet or orthopyroxene; inclusions are somewhat richer in Fe³⁺, Mg and Mn

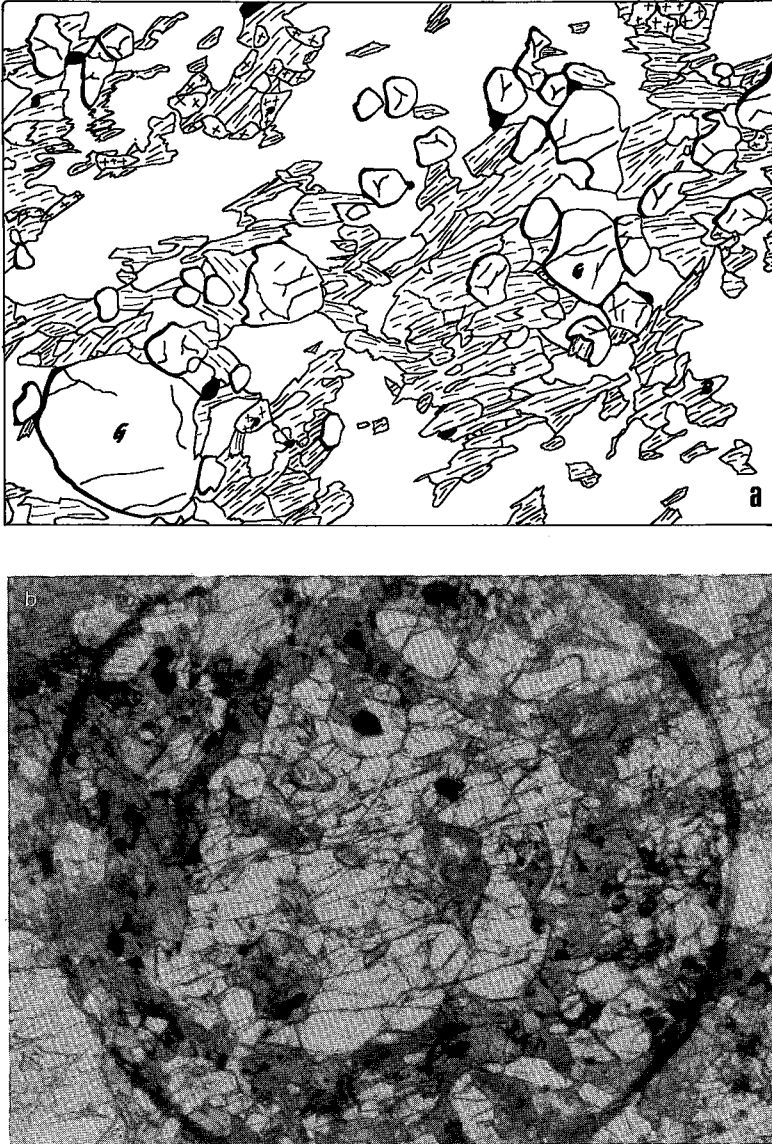
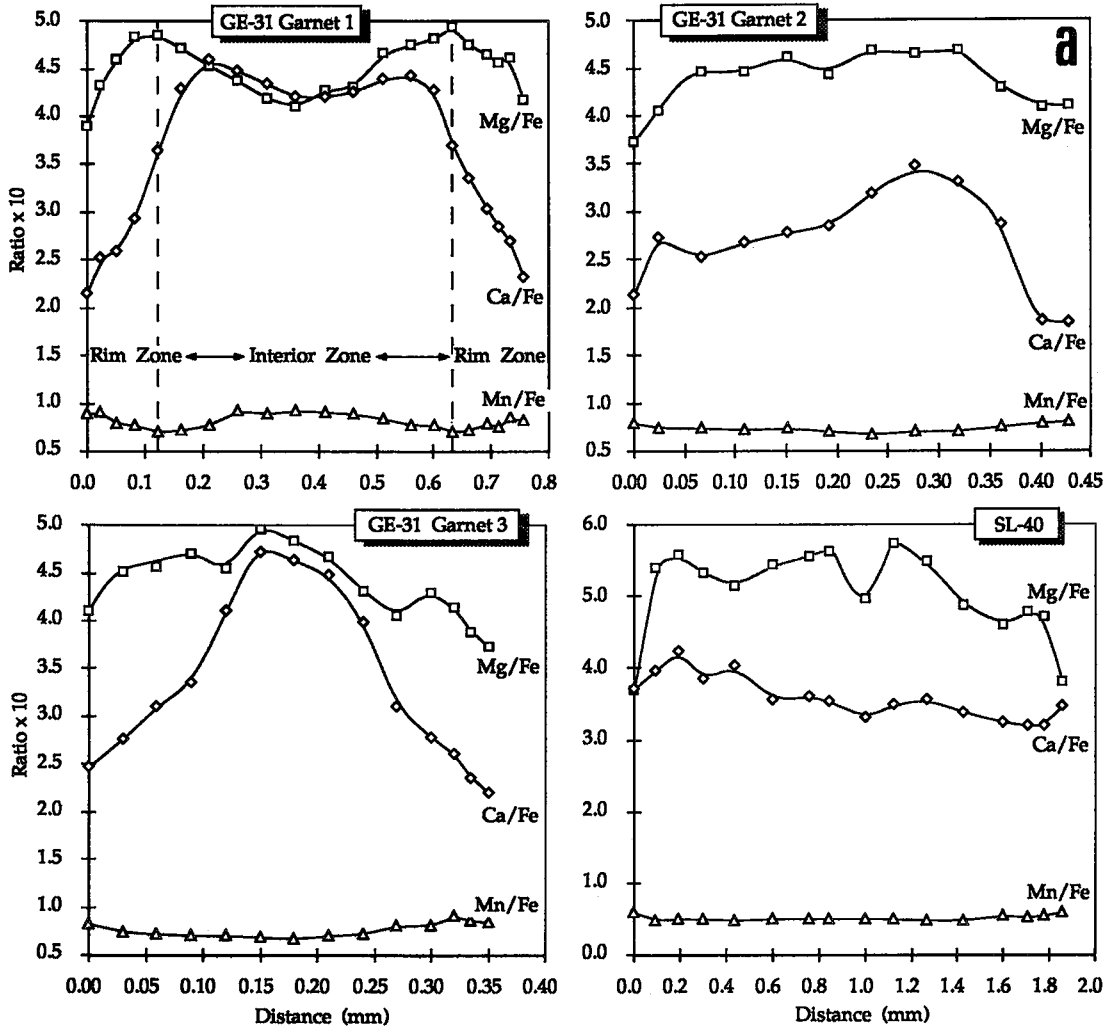


FIG. 4. Mineral textures in thin section. a. Drawing of microscopic textures in Moldanubia sample GE-31. Mineral symbols are as in Fig. 3. Field of view ~ 7 mm. b. Photo (plane-polarized light) of sample SL-40 showing textures of clinopyroxene, amphibole, plagioclase, and quartz both inside and outside of a large garnet porphyroblast (encircled). Field of view ~ 4 mm.

than matrix grains. Rutile is most commonly found as garnet inclusions.

Amphibolite sample GE-SL-40A/2 ("SL-40") belongs to a series of gneisses and amphibolites that accompany the granulites of Sankt Leonhard. They outcrop along the Steinegg - Sankt Leonhard road, about 1.5 km south of Steinegg village. Foliation is almost lacking. The mineral assemblage is $\text{grt} +$

$\text{cpx} + \text{hbl} + \text{pl} + \text{qtz} + \text{ilm} + \text{rt} + \text{ap} + \text{zrn}$ (Fig. 4b, c). Calcite and titanite occur only as minute inclusions in garnet. Secondary minerals are abundant, including green chlorite, sericite, bleached hornblende and prehnite. Despite this alteration, the original high-temperature granoblastic textures and triple junctions between hornblende, clinopyroxene, plagioclase, and quartz



are locally well preserved. Garnet is typically ~3 mm in diameter; other minerals are less than 1 mm across. Quartz is present but rare.

Garnet forms subhedral poikiloblasts, occasionally with a strongly resorbed rim. Inclusions vary in size from minute calcite and titanite grains (concentrated in the core) through larger amphibole, rutile and ilmenite grains (concentrated in the rim) to 1 mm plagioclase and clinopyroxene grains (evenly distributed throughout). Figure 5b shows these inclusion relationships schematically, as well as contours of X_{Mg} within the garnet, and points used for microprobe analysis. Figure 5a shows a compositional profile across the same grain of garnet. Except for a narrow rim, the garnet is reasonably homogeneous, although the contours of X_{Mg} in Figure 5b are rather more "disturbed". This

may be due to varying degrees of retrograde exchange with clinopyroxene and amphibole inclusions. Contours of X_{Ca} (not shown) are more regularly shaped and seem to be unaffected by retrograde reaction with plagioclase inclusions. The latter typically are inversely zoned in the range An_{44-49} (matrix: An_{48-51}), with "relict" cores of some inclusion and matrix grains reaching An_{22} and An_{14} , respectively. The most anorthite-rich (An_{54}) matrix grains are found directly adjacent to garnet.

Clinopyroxene grains typically have an Na- and Al-enriched, optically lower-index core, with exsolution lamellae too thin for resolution with the microprobe. Cpx inclusions in garnet have slightly higher X_{Mg} than matrix grains. Brown hornblende is very abundant in the rock matrix, as well as in outer portions of garnet porphyroblasts; it is

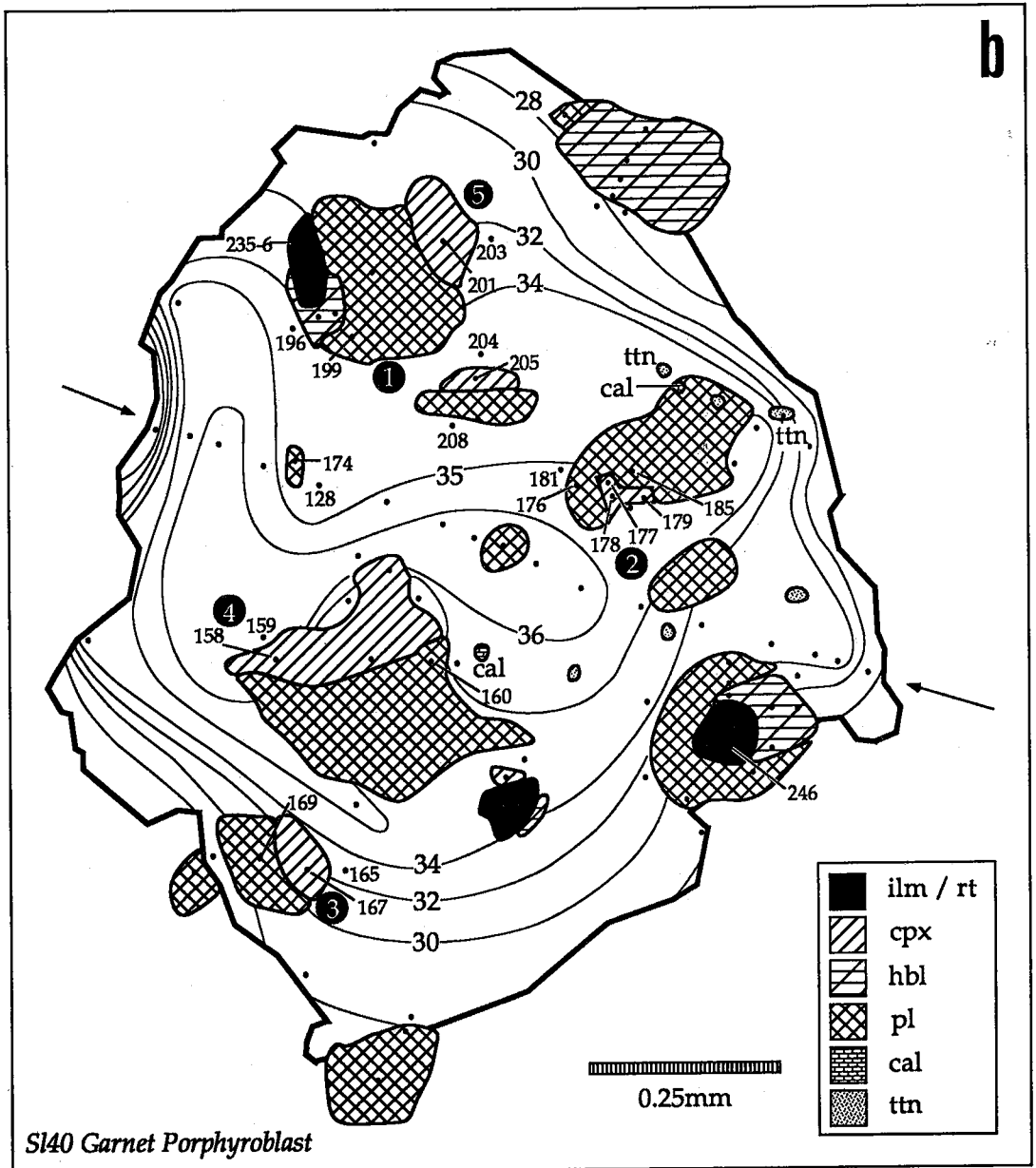


FIG. 5. Plots of garnet composition. a. Compositional profiles of three (1 large, 2 small) garnet porphyroblasts from GE-31, and the large garnet porphyroblast of sample SL-40. Y-axis values are 10 x the molar ratios Mg/Fe, Ca/Fe, and Mn/Fe, respectively. b) Schematic drawing of SL-40 garnet porphyroblast. Mineral symbols as shown. Arrows refer to the profile shown in Fig. 5a. Numbers are keyed to the individual compositions reported in Tables 2-7.

reasonably uniform in composition and appears texturally to be younger than garnet and clinopyroxene. Ilmenite and rutile occur both as garnet

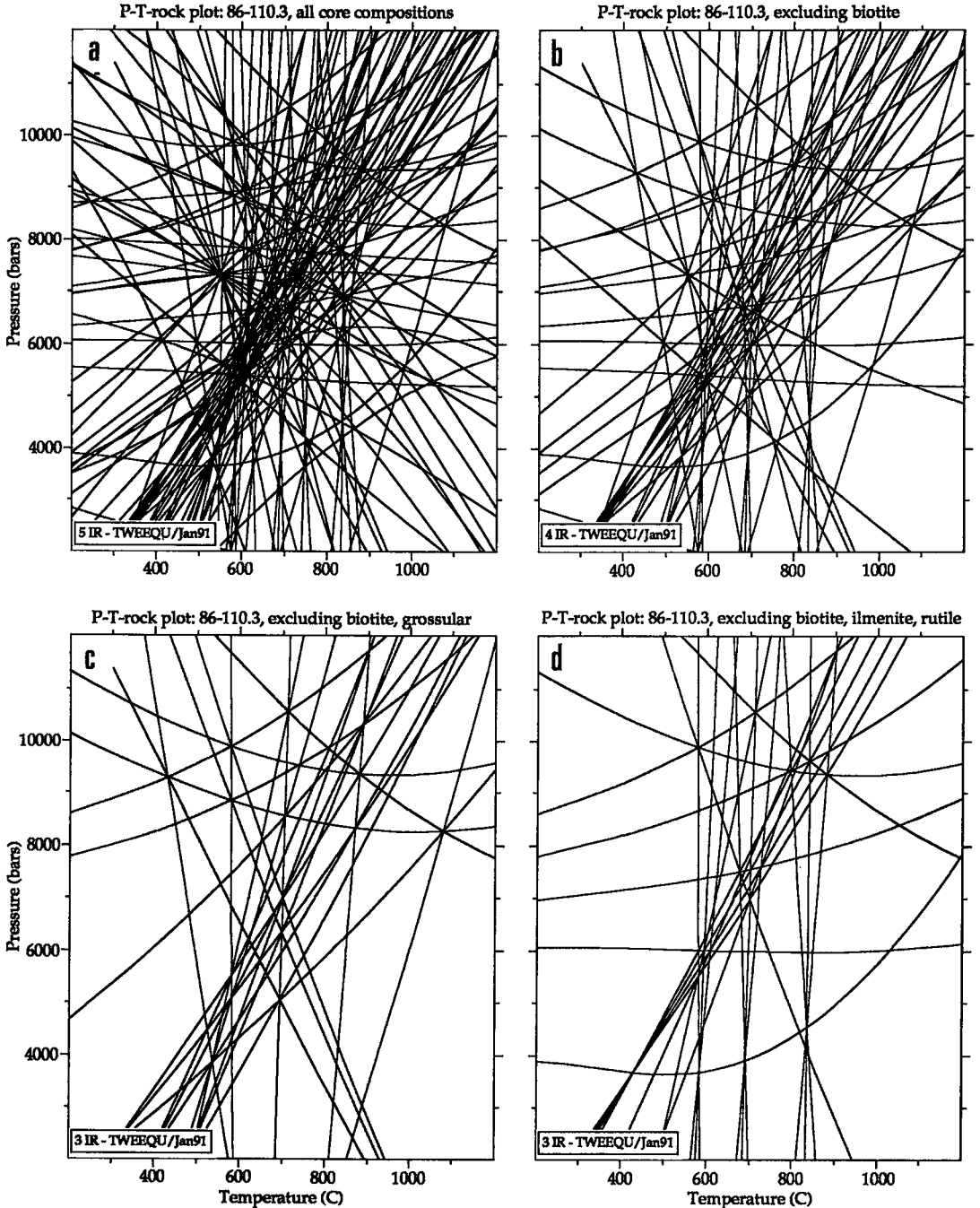
inclusions and in the matrix, although rutile is most common as inclusions. Small modal amounts of quartz, apatite, and zircon occur in the matrix.

P-T-ROCK PLOTS

86-110.3

P-T-rock plots for this sample using core mineral compositions (excluding amphibole) are

shown in Figures 6a-e, in a sequence one might typically follow in attempting to assess critically a P-T determination. The discouraging results of Figure 6a are not uncommon when one attempts to include biotite in the calculation for granulites, even when nonideal mixing of extra components in



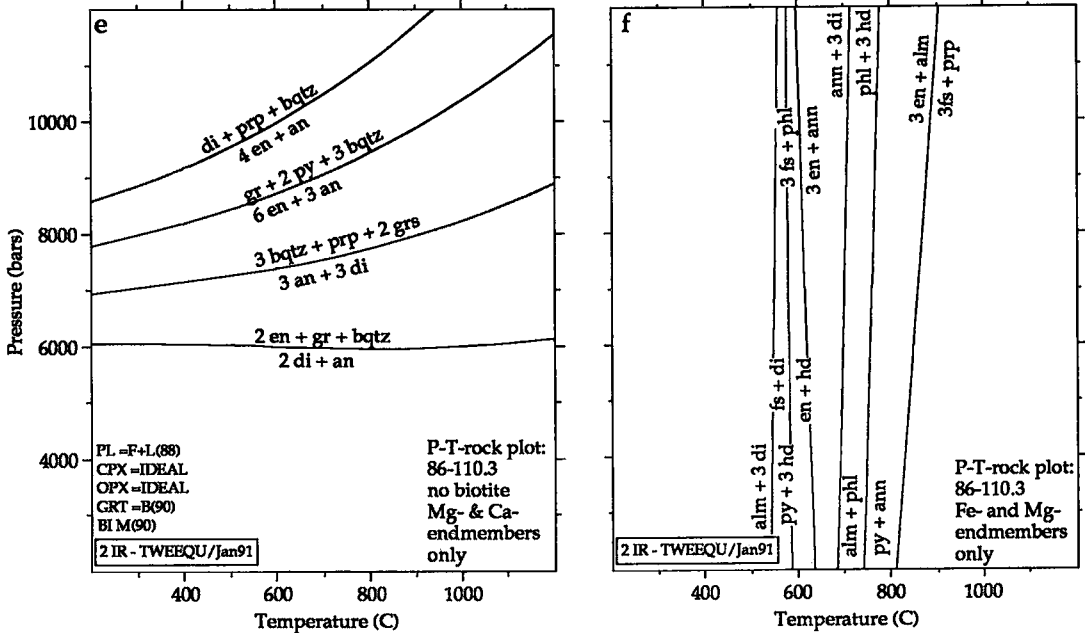


FIG. 6. P-T-rock plots for Kigluai sample 86-110.3. a) Plot of complete assemblage $\langle grs-alm-prp \rangle - \langle di-hd \rangle - \langle en-fs \rangle - \langle an-bqtz-(phl-ann) - ilm-rt \rangle$. Solution models: grt - Berman (1990), pl: Fuhrman & Lindsley (1988), bt: McMullin *et al.* (1991), opx, cpx, ilm: ideal site-mixing of cations. b) Plot excluding biotite (ann-phl). c) Plot excluding (phl-ann), grs. d) Plot excluding (phl-ann), ilm, rt. e) Plot only of Mg- and Ca-endmembers, excluding (phl-ann), alm, hd, fs, ilm, rt. f) Plot only of Mg- and Fe-end members, excluding an, grs, bqtz, ilm, rt.

biotite such as Ti and ^{VI}Al is accounted for (McMullin *et al.* 1991). A likely culprit is the low modal abundance of biotite in granulites in general, and in this sample in particular. Biotite is already, on grounds of relative diffusivity, the ferromagnesian mineral most likely to be involved in retrograde reactions: the lower the relative modal abundance of biotite, the greater the degree of compositional change it will undergo during retrogression.

Figure 6b, which excludes biotite, does not show greatly improved convergence. Clearly there are other problems. In Figure 6c, grossular is selectively excluded, on the grounds that it is the garnet component with the lowest mole fraction, and hence the greatest sensitivity to problems in the activity coefficient. This does not improve convergence significantly, nor does Figure 6d, in which ilmenite and rutile have been excluded (resulting in a complementary set of equilibria to that of Figure 6c). Suspicion that blame lies with the sample itself leads to Figure 6e, in which only reactions relating Mg-Ca end-members of the mineral assemblage are plotted, and Figure 6f, in which only Fe-Mg exchange equilibria are plotted. It seems clear at last that retrograde exchange of Fe and Mg has

occurred between at least two of the phases in the rock, causing the exchange equilibria to scatter. Whereas the progress of net-transfer reactions may have ceased near the maximum temperature, the effect of continued Fe-Mg exchange has been to alter, in a coherent fashion, the compositions of the phases analyzed and hence the computed activities of the end members of minerals involved in the net-transfer equilibria. *None* of the computed equilibria can be taken *a priori* to indicate a state of equilibrium in the rock, and so none can provide a reliable P-T estimate.

The process of re-equilibration can still be inferred, however, by assuming that the P-T estimate cited earlier (800°C, 8 kbar) is correct. The order of decreasing X_{Mg} in this sample is clinopyroxene > biotite \approx amphibole > orthopyroxene > garnet. Increasing fractionation among the phases upon cooling would have tended to drive the clinopyroxene to more Mg-rich, and the garnet, to more Fe-rich compositions. Directions of change in the other minerals would then have depended on their relative modal abundance and relative diffusivity. The observed scatter of equilibria can be explained by retrograde exchange among clinopyroxene, orthopyroxene and biotite,

with garnet taking little or no part. Curiously, the most "accurate" thermometer from this point of view is grt-bt, but a plot of all the thermometer equilibria makes clear that the biotite (\pm amphibole) compositions are most likely to have been controlled during cooling by exchange with the pyroxenes to either side in the Fe-Mg spectrum. Lack of preserved equilibration with garnet means that the "accurate" temperature estimate is only a fortuitous one.

One can infer, in addition, that clinopyroxene closed to Fe-Mg exchange before orthopyroxene, since the opx-bt equilibrium lies at a lower temperature than cpx-bt. However, the net-transfer equilibrium involving enstatite alone lies at a higher pressure than that involving diopside alone. Since the whole pattern of scatter can be explained on the basis of pressure-insensitive Fe-Mg exchange, no information on the direction of the metamorphic P-T path can really be extracted from this sample. Most likely, given the relatively minor Fe-Mg zoning of the garnet, the breakdown of garnet to symplectite shown in Figure 3a occurred at or near the maximum temperature during decompression, but the small grain-sizes of amphibole and pyroxene in the symplectite enhanced the ease of retrograde exchange.

86-117.4

P-T-rock plots for this sample are shown in Figure 7, and applicable equilibria (excluding biotite) are listed in Table 8. The clean granoblastic textures and lack of secondary alteration shown in Figure 3b suggest a good preservation of high-temperature equilibration. The plot of the complete assemblage in Figure 7a again shows a large scatter of equilibria, but this time with a pronounced central clustering. Exclusion of biotite in Figure 7b brings a marked improvement. Although biotite in this sample looks texturally as if it were fresh and unaltered, its low modal abundance in this sample would have made it particularly prone to retrograde compositional change. In Figure 7b, it is clear that most intersections lie within a relatively restricted region of 700-800°C and 6.5-9 kbar. From this diagram, one could calculate a reasonable average pressure and temperature and be done. As in the "new math", however, the point of the present exercise is not so much to extract the "correct" pressure and temperature as it is to understand what causes the equilibria to be scattered as they are. Figure 7c attempts further to reduce the scatter by excluding hedenbergite, which is involved in equilibrium no. 11 (Table 8) and whose thermodynamic properties are not that well constrained by available phase-equilibrium experiments (Ber-

man 1988). Surprisingly, this makes little difference. Equilibrium no. 19 (Table 8) is still particularly far from the others. However, exclusion of grossular rather than hedenbergite in Figure 7d results in a tight convergence at 740°C, 7.25 kbar, with three equilibria linearly independent.

Why should grossular be a problem species here? Garnet in this sample is relatively rich in the grossular component (Table 3), unlike that in many pelites. Another possibility might be its involvement in equilibria with a relatively low ΔS_r , as such equilibria are particularly sensitive to small changes in phase composition or activity (Berman 1991). Inspection of Table 8 shows that this is not the case: equilibria excluding grossular are generally lower in ΔS_r , and eq. 19 itself has a ΔS_r (42 J/deg-mol) larger than the median value in Table 8. However, many of the equilibria involving grossular do have miniscule values of ΔV_r . Such equilibria are also particularly sensitive to inaccuracy or imprecision in the activities of participating mineral species. In practice (the old math), forming an average of the intersections in Figures 7b or 7c, weighted according to the magnitudes of ΔS_r and ΔV_r as advocated by Berman (1991), leads to virtually the same P and T as in Figure 7d. Equilibria with small ΔS_r or ΔV_r , such as no. 7 or no. 9, are not necessarily widely dispersed in a particular diagram, and their close intersection in a cluster with three independent equilibria is a sensitive test of whether the thermobarometric conditions are being met. Still, in light of this sensitivity to variation in calculated activities, we will consider below whether the P-T conditions inferred from this sample are significantly different from the higher values cited earlier.

88-GE-31

A P-T-rock plot for this sample (full assemblage excluding biotite) is shown in Figure 8a. A list of the equilibria appears in Table 9. The tight convergence (706°C, 8.27 kbar) is a confirmation of the clean mineral textures suggestive of equilibrium that are seen in Figure 4a. There are three independent equilibria in this diagram, so that convergence of all the equilibria is a valid test of equilibration, but convergence of most subsets of these equilibria would not be. Equilibrium no. 3 lies farthest from the central cluster of intersections and also has the lowest ΔS_r of the set, as one might expect.

How sensitive is the convergence for this sample to other possible changes the input data? In Figure 9, three P-T-rock plots have been calculated using the same phases and compositions as in Figure 8a;

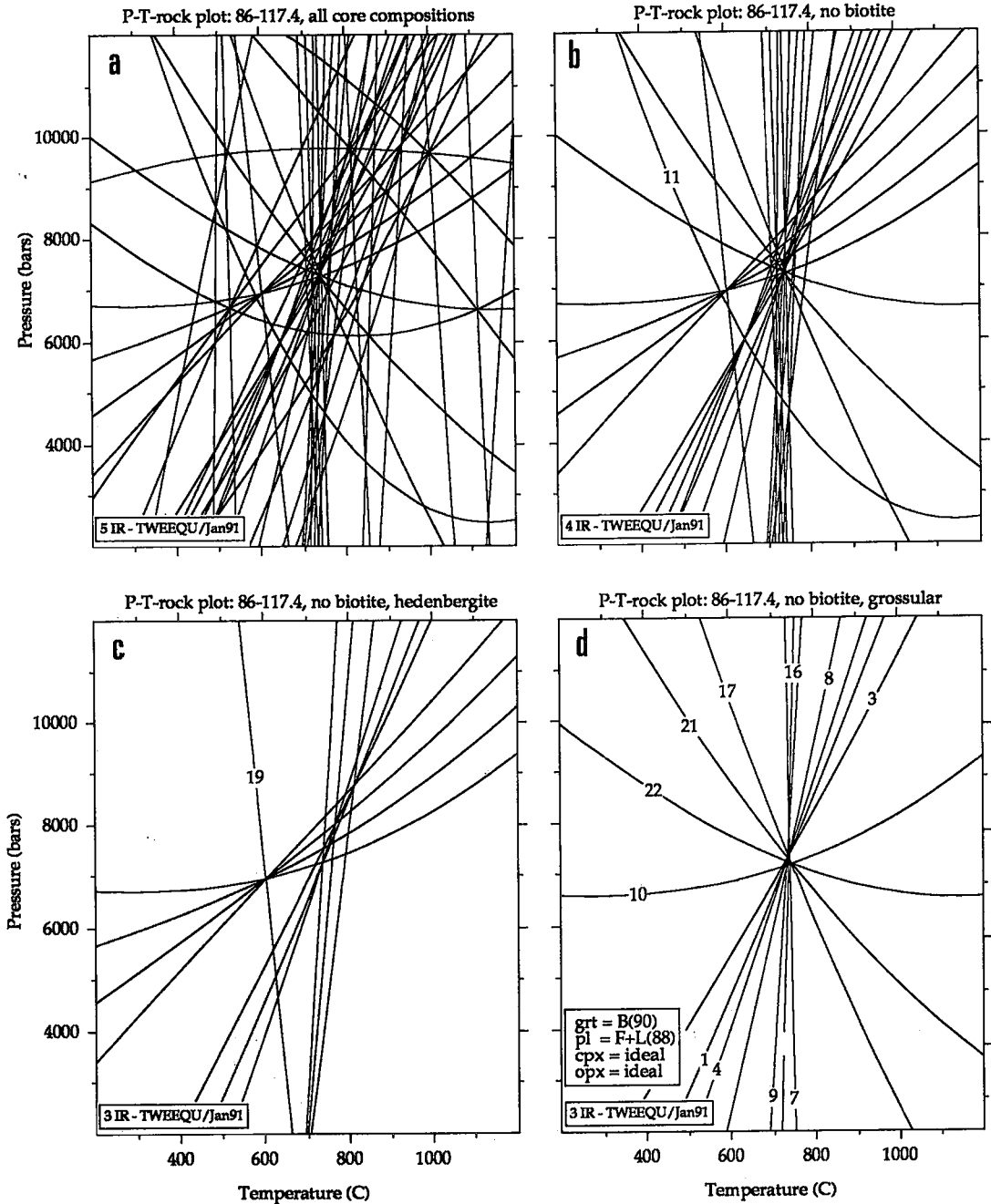


FIG. 7. P-T-rock plots for Kigluak sample 86-117.4. a) Plot of complete assemblage $\langle(\text{grs}-\text{alm}-\text{pyr}) - (\text{di}-\text{hd}) - (\text{en}-\text{fs}) - \text{an}-\text{bqtz}-(\text{phl}-\text{ann})\rangle$. Solution models as in Fig. 6. b) Plot excluding biotite ($\text{ann}-\text{phl}$). c) Plot excluding ($\text{phl}-\text{ann}$), hd . d) Plot excluding ($\text{phl}-\text{ann}$), grs . Numbered equilibria correspond to those listed in Table 8.

however, the end-member thermodynamic data were taken from Holland & Powell (1990) instead of from Berman (1988, 1990). A different activity-

composition model for garnet was employed in each diagram. In this case, choice of garnet model clearly has a much greater effect on convergence

TABLE 8. POSSIBLE EQUILIBRIA FOR SAMPLE 86-1174 (EXCLUDING BIOTITE)

No.	Equilibria	ΔS°_r (J/deg-mole)	ΔV°_r (J/bar-mole)
1	bqtz + di + alm = an + en + 3 fs	27.29	2.60
2	2 alm + grs + 3 bqtz = 6 fs + 3 an	108.07	7.33
3	bqtz + hd + alm = an + 4 fs	25.17	2.58
4	3 bqtz + 3 di + 4 alm = 3 an + 12 fs + prp	97.36	8.08
5	3 di + alm = 3 en + 3 fs + grs	26.20	0.45
6	bqtz + grs + 2 en = an + 2 di	53.49	2.14
7	hd + en = di + fs	-2.12	0.01
8	bqtz + 4 di + alm = an + 4 en + 3 hd	33.65	2.63
9	alm + 3 en = prp + 3 fs	15.49	0.29
10	bqtz + prp + di = an + 4 en	11.80	2.30
11	3 hd + alm = 6 fs + grs	-32.56	0.42
12	alm + 2 grs + 3 bqtz = 3 hd + 3 an	140.63	6.91
13	bqtz + grs + 2 fs = an + 2 hd	57.73	2.16
14	2 alm + 3 di = prp + grs + 6 fs	10.71	0.75
15	3 bqtz + prp + 2 grs = 3 an + 3 di	118.78	6.58
16	alm + 3 di = prp + 3 hd	21.85	0.33
17	bqtz + prp + 4 hd = an + 3 di + 4 fs	-3.32	2.25
18	6 di + alm = 6 en + grs + 3 hd	19.84	0.49
19	prp + 3 di = 6 en + grs	-41.69	0.16
20	grs + 2 prp + 3 bqtz = 6 en + 3 an	77.09	6.74
21	3 bqtz + 4 prp + 3 hd = alm + 3 an + 12 en	-13.55	6.57
22	bqtz + prp + hd = an + 3 en + fs	-9.68	2.29
23	prp + 6 hd = 3 di + 6 fs + grs	-54.40	0.09
24	alm + 6 en + grs = 2 prp + 3 hd	-63.54	0.17
25	prp + 3 hd = 3 en + 3 fs + grs	-48.05	0.12

TABLE 9. POSSIBLE EQUILIBRIA FOR MOLDAUBIA SAMPLES (W/O BIOTITE AND AMPHIBOLE)

No.	Equilibria	ΔS°_r (J/deg-mol)	ΔV°_r (J/bar-mol)
Sample GE31			
1	2 alm + grs + 3 bqtz = 6 fs + 3 an	108.07	7.33
2	3 en + alm = 3 fs + prp	15.49	0.29
3	fs + rt = bqtz + ilm	6.49	0.36
4	grs + 2 prp + 3 bqtz = 6 en + 3 an	77.09	6.74
5	3 rt + grs + 2 alm = 3 an + 3 fs + 3 ilm	127.54	8.42
6	2 alm + grs + 6 rt = 3 bqtz + 6 ilm + 3 an	147.02	9.50
7	3 rt + 3 en + alm = 3 ilm + prp + 3 bqtz	34.96	1.38
8	3 rt + prp + grs + alm = 3 an + 3 en + 3 ilm	112.05	8.12
9	3 rt + 2 prp + grs + 3 fs = 3 an + 6 en + 3 ilm	96.57	7.83
Sample SL40			
1	alm + hd + 4 rt = 3 bqtz + 4 ilm + an	51.14	4.03
2	grs + 2 ilm + 3 bqtz = 2 rt + 2 hd + an	44.74	1.44
3	4 hd + prp + 4 rt = 3 bqtz + 4 ilm + 3 di + an	-29.29	3.70
4	2 rt + grs + alm = 2 an + hd + 2 ilm	95.88	5.47
5	alm + 3 hd + 6 rt = 6 bqtz + 6 ilm + grs	6.39	2.59
6	6 rt + grs + 2 alm = 3 an + 6 ilm + 3 bqtz	147.02	9.50
7	3 bqtz + 2 grs + alm = 3 an + 3 hd	140.63	6.91
8	alm + 3 di = prp + 3 hd	21.85	0.33
9	4 alm + 3 di + 12 rt = 9 bqtz + prp + 12 ilm + 3 an	175.26	12.42
10	2 rt + prp + 2 hd + grs = 2 an + 3 di + 2 ilm	-74.04	5.14
11	6 rt + prp + 6 hd = 3 di + grs + 6 ilm + 6 bqtz	-15.45	2.26
12	3 bqtz + prp + 2 grs = 3 an + 3 di	118.78	6.58
13	6 rt + prp + 3 grs + 2 alm = 6 an + 3 di + 6 ilm	265.80	16.09
14	2 alm + 3 di + 6 rt = 6 bqtz + prp + 6 ilm + grs	28.24	2.92

than choice of data-set. Figure 9a shows very good convergence, and much of the remaining scatter may in fact be due to the lack of internal consistency between end-member data and garnet

solid-solution parameters. However, equilibrium 3 is significantly more off track than in Figure 8 and involves no garnet. This detracts very little from the quality of the P-T determination in question,

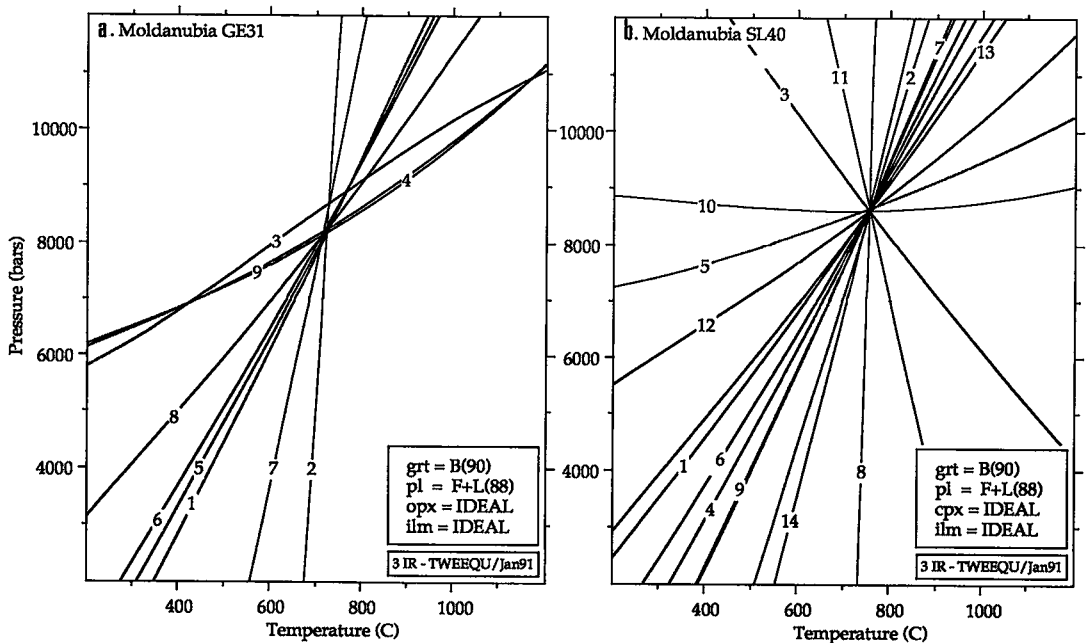


FIG. 8. P-T-rock plots for Moldanubia samples GE-31 and SL-40. Numbered equilibria correspond to those listed in Table 9. a) Plot of complete GE-31 assemblage (grs-alm-prp) - (en-fs) - an-bqtz-ilm-rt, excluding biotite. Solution models as in Fig. 6. b) Plot of complete SL-40 assemblage (grs-alm-prp) - (di-hd) - an-bqtz-ilm-rt, excluding biotite. Solution models as in Fig. 6.

P-T-rock plots: Moldanubia GE-31 core compositions and thermo-data of Holland and Powell (1990)

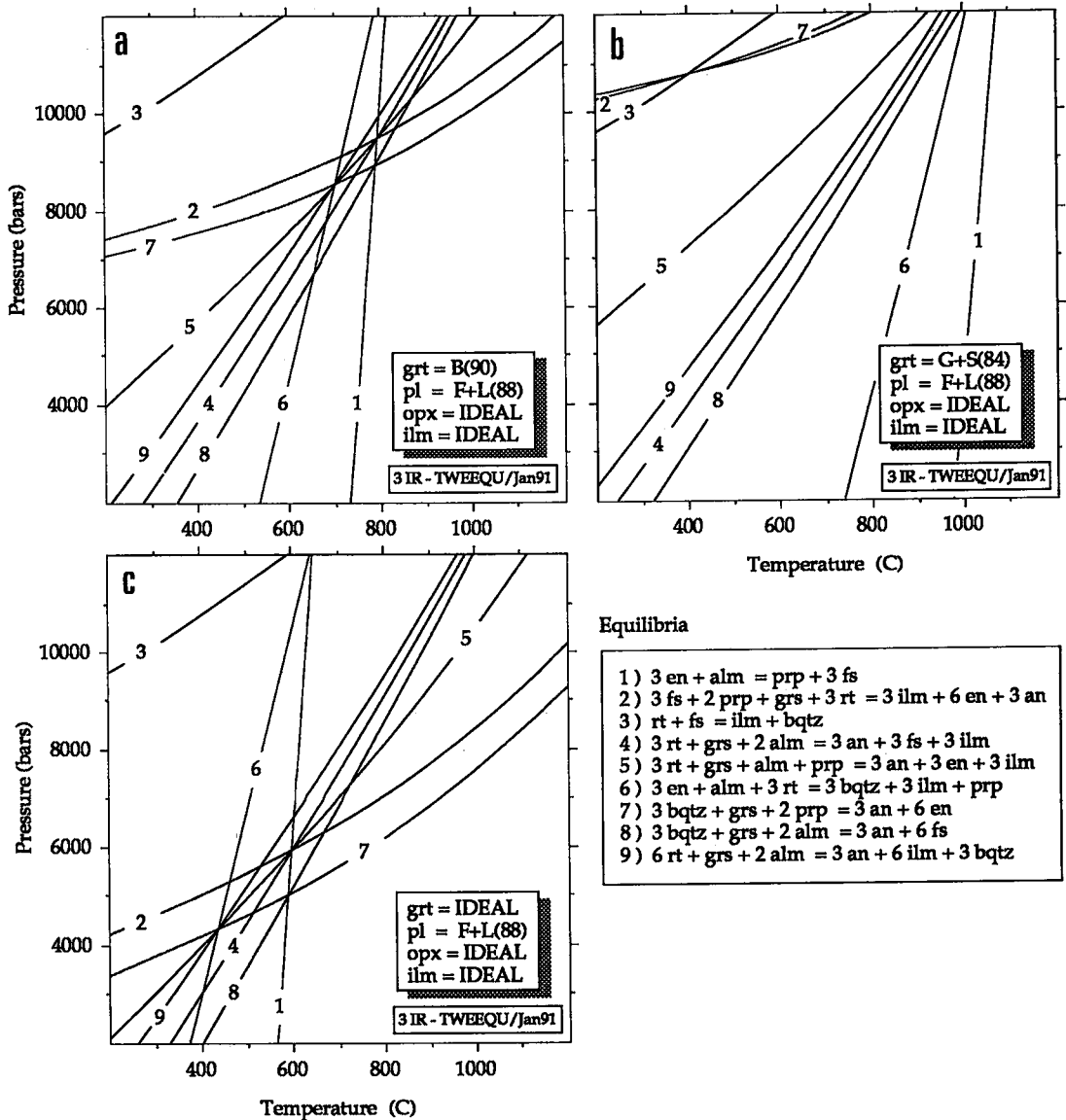


FIG. 9. P-T-rock plots for Moldanubia sample GE31. Assemblage as in Fig. 8a, but utilizing the thermodynamic data-set of Holland & Powell (1990) with three different solution-models for garnet: a) Berman (1990); b) Ganguly & Saxena (1984); and c) ideal site-mixing of cations. Only c) is truly consistent with this data-set.

but illustrates an important point. Despite apparently small numerical differences between the two major thermodynamic data-sets, the exceedingly sensitive test of convergence in a P-T-rock plot can often clearly differentiate between them. In

more general terms, application of this test is a very effective tool for evaluation and refinement of any and all of the information that goes into thermobarometry. Included in this information are thermodynamic data, formulations for solution

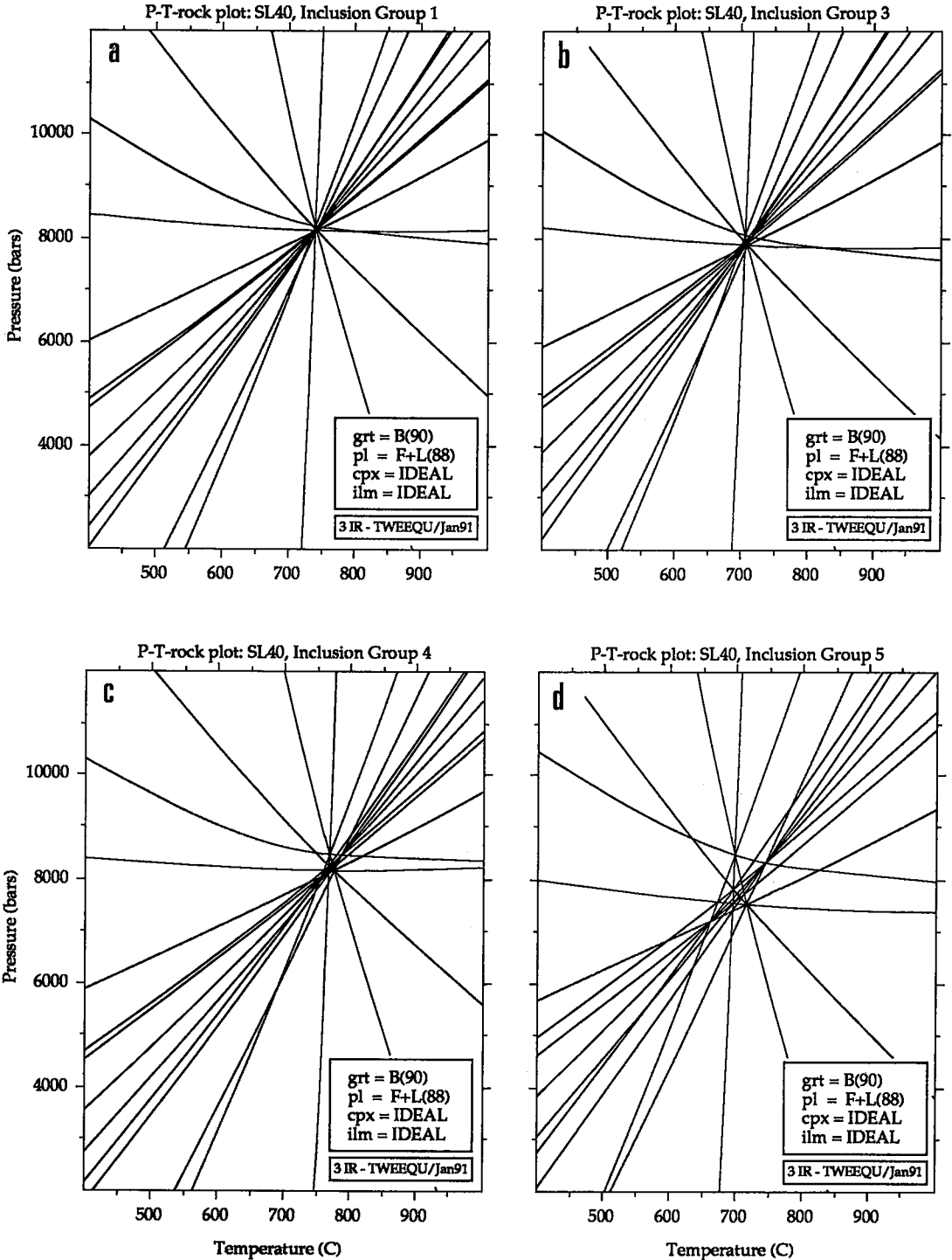


FIG. 10. P-T-rock plots for Moldanubia sample SL40. Shown are plots of the assemblage <(grs-alm-prp) - (di-hd) - an-bqtz-ilm-rt> using analyzed compositions from four separate groups of included minerals in the garnet. Numbers of inclusion groups are keyed to those in Fig. 5b. Solution models as in Fig. 6.

models, analytical techniques, and also the suitability of samples in terms of their modal compositions.

GE-SL40A/2

A P-T-rock plot for core compositions of all major minerals in the matrix of this sample except amphibole is shown in Figure 8b; equilibria are listed in Table 9. Despite the appearance in thin section of textural evidence for alteration and retrogression (Fig. 4b), a tight convergence is obtained at 740°C, 8.25 kbar. For this paragenesis as well, the equilibrium most widely displaced from the central cluster (no. 5) has the lowest ΔS_r .

Our initial hypothesis was that some of the groups of included minerals shown in Figure 5b might better preserve a state of equilibrium than grains in the matrix outside the garnet, owing to protection by the garnet porphyroblast. P-T-rock plots for four such groups are shown in Figure 10. The first three groups of inclusions give results virtually identical to those for matrix minerals. The plot for group 5 is more disturbed, yet the dispersion of equilibria is very much in line with the relative ΔS_r values shown in Table 9. Weighted average pressures and temperatures for all plots are virtually indistinguishable. The tempting conclusion is that the variations seen in Figure 10 are simply the result of analytical uncertainties. This type of hypothesis is particularly well suited to testing by means of the Monte Carlo simulations discussed below.

MONTE CARLO SIMULATIONS

Permutated P-T-rock plots

Shown in Figure 11 are six P-T-rock-plot permutations for the sample SL-40, for the paragenesis defined as the cores of mineral grains not included in garnet. The equilibria most variable in position from plot to plot are again those with the lowest ΔS_r . A comparison with Figure 10 shows that the style as well as the extent of variability from one inclusion group to another agree quite well with those to be expected from analytical imprecision, even were the "true" mineral compositions to be identical from group to group. In this case, all of the apparent variation in quality of convergence could reasonably be assigned to analytical uncertainties rather than to varying degrees of re-equilibration.

Even though the analyzed variability in mineral compositions within a thin section is frequently greater than the nominal 1% (relative) employed in the simulation (Tables 2-7), such variability does

not express the very substantial negative correlations present in compositions of the minerals analyzed. It is entirely possible (although not inevitable), as this example shows, that highly correlated 2-3% uncertainties, resulting from sample inhomogeneity, can produce uncertainties in pressure and temperature that are very similar to those obtained from uncorrelated 1% counting uncertainties.

Intersection plots

In Figure 12 are plotted all P-T intersections from 100 P-T-rock-plot permutations for each of the samples 86-117.4, GE-31, and SL-40. Since each plotted intersection is a potentially correct P-T determination resulting from potentially correct analytical values, each of the three populations of plotted points ($n \approx 8000$) is an accurate representation of the effect of analytical uncertainties on P and T calculated from any single intersection. For each sample, the spread of points is disconcertingly large, and P and T are strongly correlated (SL-40; $\rho = 0.84$); these results are similar to those derived by Hodges & McKenna (1987). The strong correlation between P and T for sample 86-117.4 means that the differences between 800°C, 8 kbar, the conditions cited earlier for the peak metamorphic temperature, and those derived in this report (740°C, 7.25 kbar), can be reconciled, within 2σ uncertainty, on the basis of analytical variability. Not clear in these figures, owing to the large number of points, is that each plot does have a very well-defined central tendency. A number of methods of calculating mean P and T all yield very close to the same values as those of the unperturbed plot.

In Figure 13, pressures and temperatures from the intersections for sample SL-40 have been plotted against the expected cumulative frequency for normal distributions. The large numbers of extreme points show up clearly in the curved ends of each plot. The non-normal "tail-heavy" distributions and high correlation mean that simply reporting values of P and T plus or minus a standard deviation will not express the likelihood of a particular P and T being the "true" value, nor the likelihood that two P-T determinations are significantly different. Neither is it true that probability contours for two variables will necessarily take the form of ellipsoids or sums of ellipsoids.

A direct method of displaying confidence regions about an x-y point is to construct contours of equal areal density for the simulated population of points. This has been done for the P-T points from sample SL-40 (Fig. 14). Approximately 10% of the

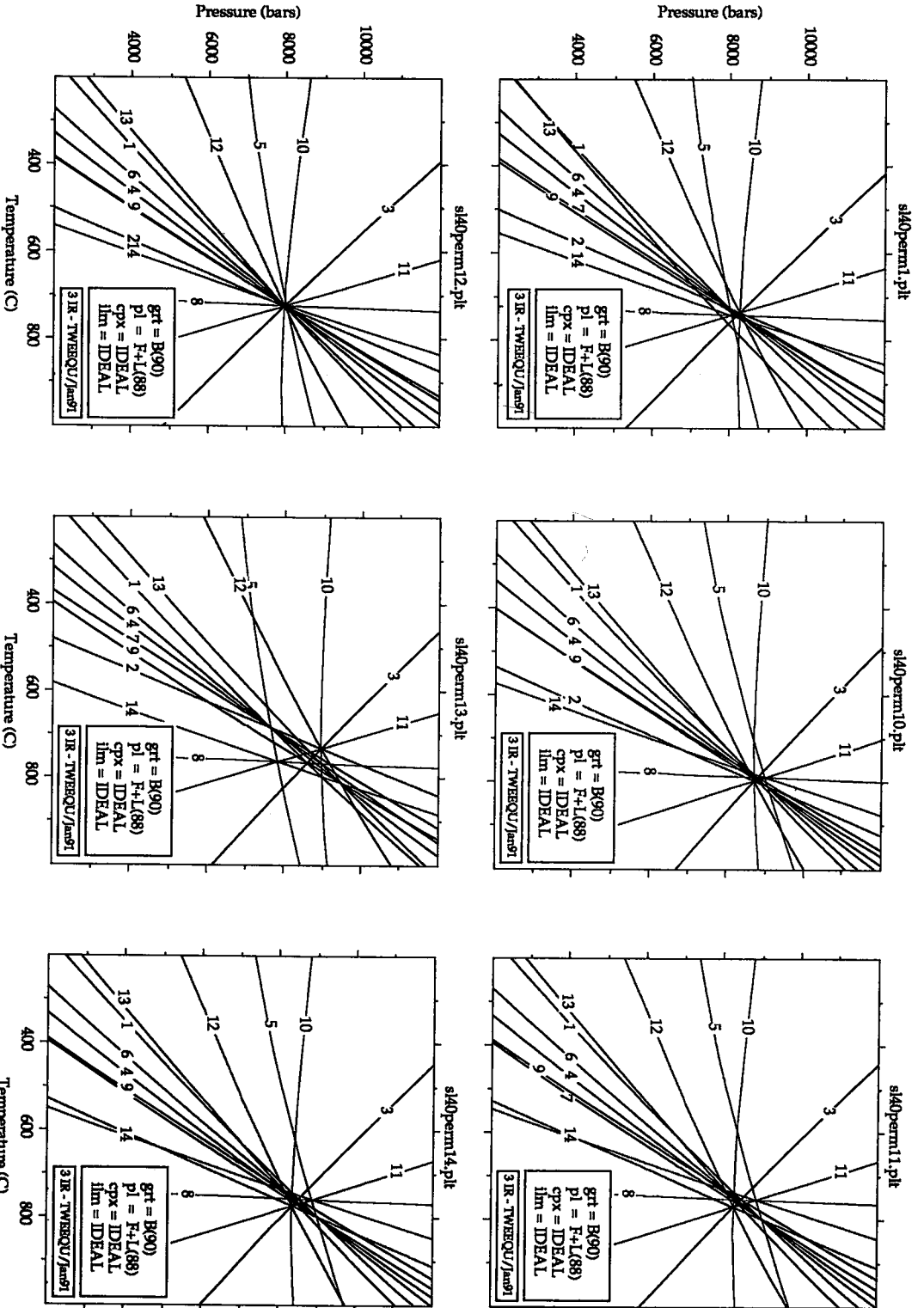


FIG. 11. P-T-rock plots for Moldanubia sample SL40. Shown are plots of the assemblage <(grs-alm-prt) - (di-hd) - an-bqtz-ilm-rt> using five different permutations of the average core compositions of matrix minerals (original = sl40perm1). Solution models as in Fig. 6.

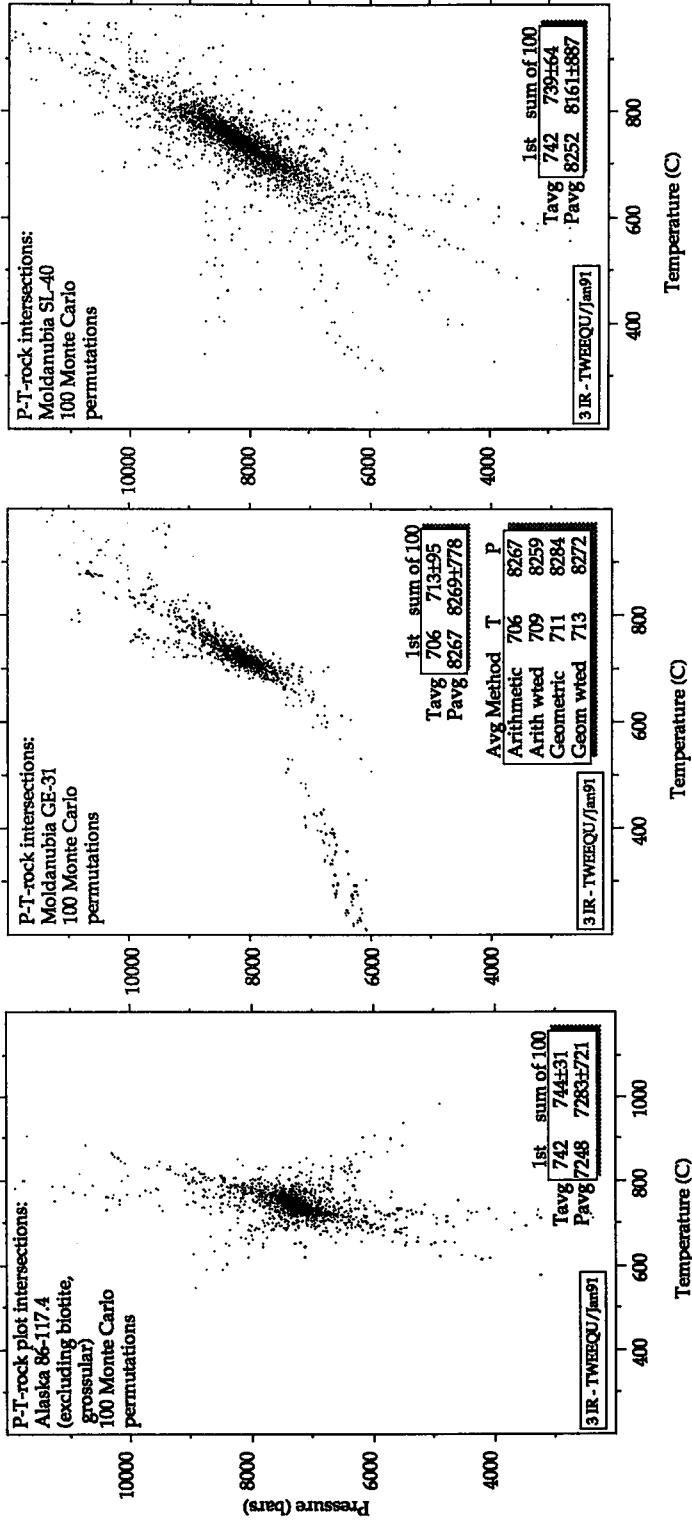


FIG. 12. P-T-rock intersection plots. Plotted are all reaction intersections for all 100 permuted sets of mineral composition. Shown are mean P and T for the analyzed compositions *versus* those for all permutations; they are not significantly different. For sample CE-31, several different methods of calculating mean P and T are shown: arithmetic or geometric, with or without down-weighting of acute intersections. The different methods of averaging yield similar results when the mean values are already so closely constrained as here.

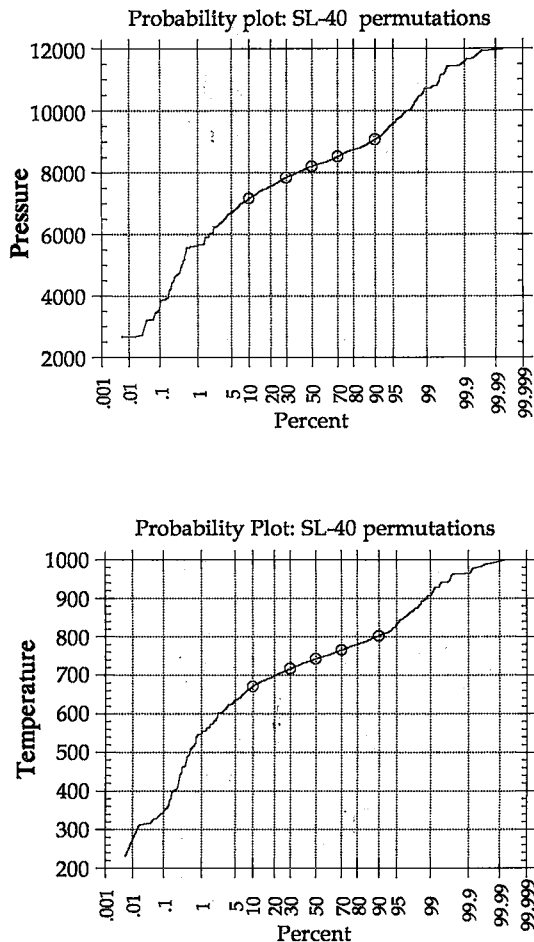


Fig. 13. Normal probability plots for temperature and pressure using the set of Monte Carlo P-T points for SL-40 shown in Fig. 12. A normal (gaussian) distribution of values in this diagram would plot on a straight line. Both P and T are "heavy-tailed", with many more outlying values than would be expected from a normal distribution.

most extreme points have been excluded. Contours are shown enclosing 5%, 65%, and 95% of the points within the bounds of the plot, constituting 5%, 65%, and 95% confidence regions in the P-T plane. Whereas the first two contours are reasonably close to ellipses, the 95% contour is much less elliptical and clearly more than twice as far from the mean pressure and temperature as the 65% contour, in reasonable agreement with the observed "tail-heavy" nature of the distribution of points.

As an improvement on the traditional " \pm " notation, these confidence regions can be used

directly to report thermobarometric results and to test petrological hypotheses. In the present example, Figure 14 makes clear that the P-T points (800°C, 9 kbar) and (750°C, 8 kbar) would not be different to a very high level of significance. One should indeed be suspicious of "P-T paths" defined by a number of samples plotting along such a trend. However, two rocks of similar mineral composition that plot at (700°C, 9 kbar) and (800°C, 7.5 kbar) could be considered very likely to have equilibrated under significantly different conditions.

Best-estimate plots

The large regions of confidence plotted in Figure 14 would certainly lead to very small confidence in any reported pressures and temperatures inferred from the thermobarometric method discussed in this report. However, it is important to remember that in any statistical analysis, the meaning of the answers depends crucially on the question. In the preceding section, we asked the question: what is the probability distribution of single P-T intersections? The answer to this question is: large, non-gaussian, highly correlated. However, with all possible equilibria at our disposal for the purpose of inferring the pressure and temperature of equilibration, we can ask a perhaps more important question: what is the probability distribution of P-T points that are themselves best estimates from entire sets of equilibria, not just single pairs of thermobarometers? The best estimate is here defined as a robust weighted average, allowing for the effects of ΔS_r , ΔV_r , and oblique angle of intersection on the variability in position of the intersection between two equilibria, as discussed above and by Berman (1991).

In Figure 15 are plotted 100 such best estimates for the same 100 data-sets as in Figure 14. A first observation is that the distribution of best estimates of pressure and temperature is much smaller than the distribution of single intersections, and perhaps even more highly correlated. The second, less obvious point comes from the Central Limit Theorem (found in any statistics text); it states that, for *any* probability distribution (gaussian or not) for which the variance is noninfinite, the distribution of averages taken from subsets of the distribution will be very close to gaussian. This means that, even though the distribution of single P-T intersections is non-gaussian, the distribution of best estimates can be well approximated by a gaussian distribution. In the present example, this conclusion enables us to calculate and plot directly an ellipse corresponding to the 2σ region of confidence about the best-estimate pressure and temperature, saving the trouble of having to

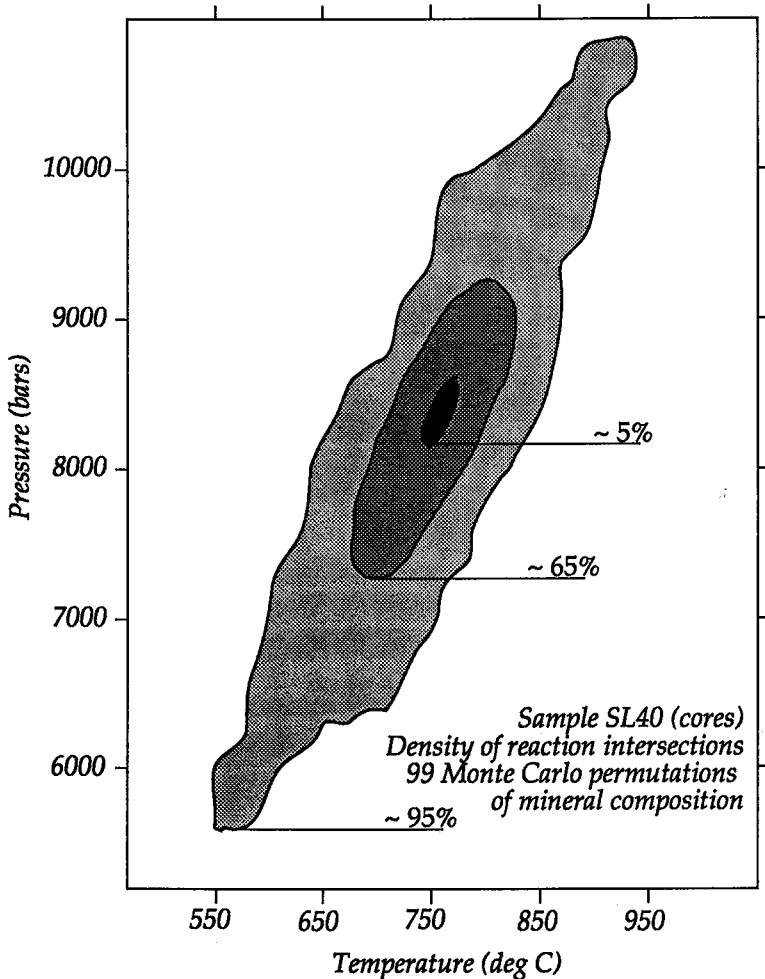


FIG. 14. Contoured P-T-rock intersection plot for sample SL-40. The accumulated intersections from Monte Carlo permutations have been contoured for areal density. The contours shown enclose, respectively, 5%, 65%, and 95% of the total P-T intersections within the plot area (~85% of the intersections shown in Fig. 12).

empirically contour the integrated probability-distribution as in Figure 14. Uncertainties in best estimates could also be accurately reported in the form of variance-covariance matrices, although plotted ellipses would still be easier to compare and to interpret.

SUMMARY AND CONCLUSIONS

The availability of dozens of geothermometer and barometer calibrations, as well as packaged computer programs to apply them, has made it relatively easy for the petrologist to calculate many

pressures and temperatures for every sample. As a result, the interpretation of this deluge of numbers has never been harder. TWEEQU thermobarometry is one means of determining not only a "best" P and T, but also of critically assessing the quality and reliability of that determination, by means that can be independent of the geological reasoning and textural assessment of equilibrium applied up to now. A valid "P-T-rock-plot" test of convergence does require, however, internally consistent thermodynamic data (end-member properties *and* solution models for minerals) of high quality for a sufficient number of the phases

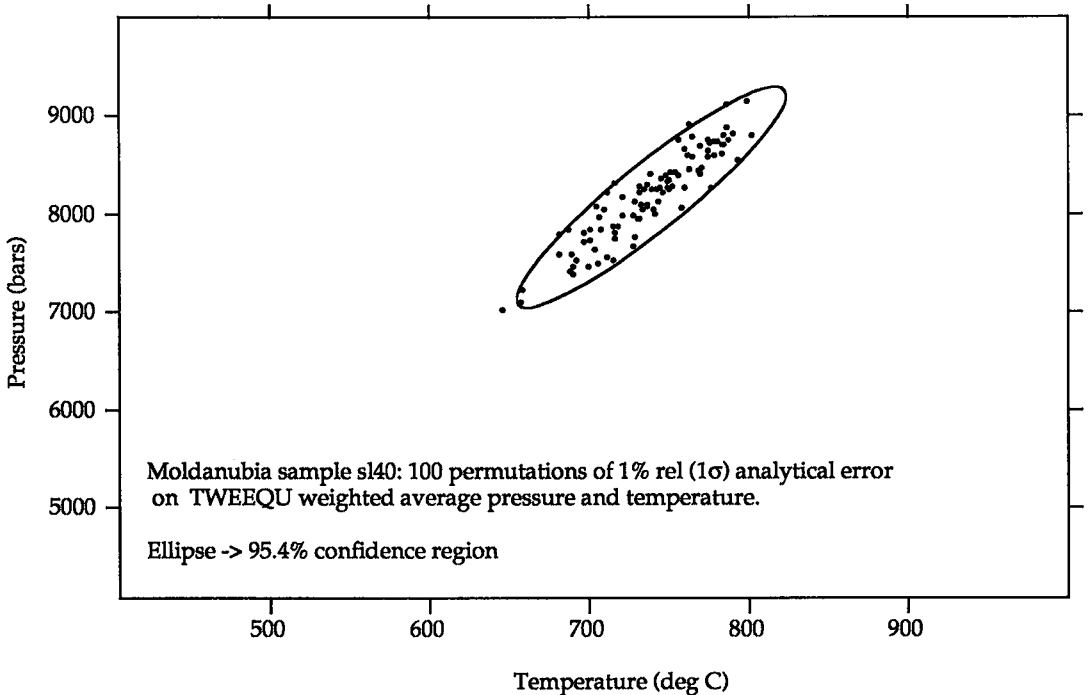


FIG. 15. Confidence ellipse (2σ) for "best-guess" P-T estimates from the 100 simulated P-T-rock diagrams for sample SL40. Each "best-guess" is an average of all intersections in a diagram, weighted according to the magnitude of ΔS_i and ΔV_i for both intersecting equilibria, as well as of the angle of intersection. Very low-angle intersections are excluded altogether from each average.

in a paragenesis to allow for at least three linearly independent equilibria.

Four garnet-pyroxene gneisses from the Kigluaik Mountains, western Alaska and the Bohemian Massif, Austria, have been used to illustrate ways of using P-T-rock plots to examine hypotheses concerning choice of phases components, choice of relevant equilibria, uncertainties in thermodynamic data, activity-composition problems, and perturbed equilibrium among minerals of observed parageneses. In some cases, but not all, such hypotheses can be accepted or rejected on the basis of sequential P-T-rock-plot calculations, which are relatively easy and fast with currently available computers and software. The test of convergence in such a plot is an extremely sensitive tool for examining the differences between sets of input conditions and data, such as thermodynamic data-sets. It can equally well be used to refine those input data. For example, optimization of the convergence for samples that are believed, on a variety of grounds, to be well equilibrated, can lead to better solution models for minerals where insufficient experimental data are available or the experiments are too difficult to carry out.

The propagation of uncertainties in input data by means of an analytical expression is neither straightforward nor appropriate for TWEEQU calculations. Uncertainties in pressure and temperature due to imprecision in electron-microprobe data, derived here by means of a Monte Carlo simulation, are both a valid and accurate determination of uncertainties due to one source of error, and a model for propagating other uncertainties, such as those to be established for thermodynamic data, through TWEEQU calculations.

One of two geological questions posed in this report can be answered in the affirmative. Both Moldanubian samples could have equilibrated under the same P-T conditions, within the limits of compositional uncertainty, suggesting that the contact between them could well be pre-metamorphic. Results on a TWEEQU analysis presented in this report cannot, however, answer the question concerning whether the Kigluaik granulites equilibrated at a range of pressures. It can only be shown by examination of the patterns of scattering among the equilibria that apparent cooling paths suggested for each sample can be as well or better

explained by retrograde Fe-Mg exchange in one sample, and variability of electron-microprobe data in the other.

On the basis of Monte Carlo calculations of uncertainties in single P-T intersections resulting from one source of error, the prospects for high-precision thermobarometry would appear dim. The picture brightens considerably if one considers instead the uncertainties attached to the best estimate one can derive from a full multi-equilibrium TWEEQU analysis. The method presented in this report can and will be extended to consider a number of other sources of error in thermobarometry. Specific petrological hypotheses can be much more readily and correctly tested where calculated regions of confidence associated with P-T estimates are reported in graphical form (*i.e.*, as plotted ellipses) rather than as "±" errors. One hopes that this will eventually become the accepted method of reporting thermobarometric results.

ACKNOWLEDGEMENTS

The authors acknowledge M. Engi and R.G. Berman for many helpful and enjoyable discussions. K.V. Hodges, R.G. Berman, and an anonymous reviewer contributed detailed and useful reviews. Parts of this work were supported by U.S. National Science Foundation grants EAR 8218471 and 8507757 to B.W. Evans, Schweizer. Nationalfonds grant 2.752.87-5459 to M. Engi, a Sigma Xi Grant-in-Aid to J. Lieberman, a grant from Fonds zur Förderung der Wissenschaftlichen Forschung, Austria, J0340-GEO to K. Petrakakis, and the Electron Microprobe Laboratory, University of Bern. The first author also expresses, on the occasion of this special volume, his appreciation to Hugh for encouragement and support in many dimensions.

REFERENCES

- AITCHISON, J. (1986): *The Statistical Analysis of Compositional Data*. Chapman & Hall, New York.
- ANDERSON, G.M. (1976): Error propagation by the Monte Carlo method in geochemical calculations. *Geochim. Cosmochim. Acta* **40**, 1533-1538.
- ARMSTRONG, R.L., HARAKAL, J.E., FORBES, R.B., EVANS, B.W. & THURSTON, S.P. (1986): Rb-Sr and K-Ar study of metamorphic rocks of the Seward Peninsula and southern Brooks Range, Alaska. *In* Blueschists and Eclogites (B.W. Evans & E.H. Brown, eds.). *Geol. Soc. Am., Mem.* **164**, 185-203.
- BENCE, A.E. & ALBEE, A.L. (1968): Empirical correction factors for the electron micro-analysis of silicates and oxides. *J. Geol.* **76**, 382-403.
- BERMAN, R.G. (1988): Internally-consistent thermodynamic data for minerals in the system Na₂O-K₂O-CaO-MgO-FeO-Fe₂O₃-Al₂O₃-SiO₂-TiO₂-H₂O-CO₂. *J. Petrol.* **29**, 445-522.
- (1990): Mixing properties of Ca-Mg-Fe-Mn garnets. *Am. Mineral.* **75**, 328-344.
- (1991): Thermobarometry using multi-equilibrium calculations: a new technique, with petrological applications. *Can. Mineral.* **29**, 833-855.
- , BROWN, T.H. & GREENWOOD, H.J. (1985): An internally-consistent thermodynamic data base for minerals in the system Na₂O-K₂O-CaO-MgO-FeO-Fe₂O₃-Al₂O₃-SiO₂-TiO₂-H₂O-CO₂. *Atomic Energy of Canada Ltd., Tech. Rep.* **377**.
- , BROWN, T.H. & PERKINS, E.H. (1987): GEO-CALC: software for calculation and display of pressure - temperature - composition phase diagrams. *Am. Mineral.* **72**, 861-862.
- , ENGI, M., GREENWOOD, H.J. & BROWN, T.H. (1986): Derivation of internally consistent thermodynamic data by the technique of mathematical programming, a review with application to the system MgO-SiO₂-H₂O. *J. Petrol.* **27**, 1331-1364.
- BEVINGTON, P.R. (1969): *Data Reduction and Error Analysis for the Physical Sciences*. McGraw-Hill, New York.
- CARSWELL, D.A., MÖLLER, C & O'BRIEN, P.J. (1989): Origin of sapphirine - plagioclase symplectites in metabasites from Mitterbachgraben, Dunkelsteinerwald granulite complex, Lower Austria. *Eur. J. Mineral.* **1**, 455-466.
- CHAYES, F. (1960): On correlation between variables of constant sum. *J. Geophys. Res.* **65**, 4185-4193.
- CHIPERA, S.J. & PERKINS, D. (1988): Evaluation of biotite - garnet geothermometers: application to the English River Subprovince, Ontario. *Contrib. Mineral. Petrol.* **98**, 40-48.
- ERMOLIEV, Y. & WETS, R.J.-B. (1988): Stochastic programming: an introduction. *In* Numerical Techniques for Stochastic Optimization 1 (Y. Ermoliev & R.J.-B. Wets, eds.). Springer-Verlag, Berlin (1-32).
- FUCHS, G. (1976): Zur Entwicklung der Böhmisches Masse. *Jahrb. Geol. B.-A.* **119**, 45-61.
- & MATURA, A. (1976): Zur Geologie des Kristallins der Südlichen Böhmisches Masse. *Jahrb. Geol. B.-A.* **119**, 1-43.
- & ——— (1980): Die Böhmisches Masse in Österreich. *In* Der Geologische Aufbau Österreichs (? Oberhauser, ed.). Springer, Vienna (121-143).

- ____ & SCHARBERT, G.H. (1979): Kleinere Granulitvorkommen im niederösterreichischen Moldanubikum und ihre Bedeutung für die Granulitgenese. *Verh. Geol. B.-A.*, 29-49.
- FUHRMAN, M.L. & LINDSLEY, D.H. (1988): Ternary-feldspar modeling and thermometry. *Am. Mineral.* **73**, 201-215.
- GANGULY, J. & SAXENA, S.K. (1984): Mixing properties of aluminosilicate garnets: constraints from natural and experimental data, and applications to geothermobarometry. *Am. Mineral.* **69**, 88-97.
- HODGES, K.V. & CROWLEY, P.D. (1985): Error estimation and empirical geothermobarometry for pelitic systems. *Am. Mineral.* **70**, 702-709.
- ____ & MCKENNA, L.V. (1987): Realistic propagation of uncertainties in geologic thermobarometry. *Am. Mineral.* **72**, 671-680.
- ____ & SPEAR, F.S. (1982): Geothermometry, geobarometry, and the Al_2SiO_5 triple point at Mt. Moosilauke, New Hampshire. *Am. Mineral.* **67**, 1118-1134.
- HÖGELSBERGER, H. (1989): Die Marmore und Kalksilikatgesteine der Bunten Serie – Petrologische Untersuchungen und geologische Konsequenzen. *Jahrb. Geol. B.-A.* **132**, 213-230.
- HOLLAND, T.J.B. & POWELL, R. (1990): An enlarged and updated internally consistent thermodynamic dataset with uncertainties and correlations: the system $K_2O-Na_2O-CaO-MgO-MnO-FeO-Fe_2O_3-Al_2O_3-TiO_2-SiO_2-C-H_2-O_2$. *J. Metamorph. Geol.* **8**, 89-124.
- KOHN, M.J. & SPEAR, F.S. (1991): Error propagation for barometers. 1. Accuracy and precision of experimentally located end-member reactions. *Am. Mineral.* **76**, 128-137.
- KRETZ, R. (1983): Symbols for rock-forming minerals. *Am. Mineral.* **68**, 277-279.
- KRÖNER, A., WENDT, I., LIEW, T.C., COMPSTON, W., TODT, W., FIALA, J., VANKOVA, V. & VANEK, J. (1988): U-Pb zircon and Sm-Nd model ages of high-grade Moldanubian metasediments, Bohemian Massif, Czechoslovakia. *Contrib. Mineral. Petrol.* **99**, 257-266.
- LIEBERMAN, J.E. (1988): *Metamorphic and Structural Studies of the Kigluaik Mountains, Western Alaska*. Ph.D. thesis, Univ. Washington, Seattle, Washington.
- ____ & RICE, J.M. (1986): Petrology of marble and peridotite in the Seiad ultramafic complex, northern California, USA. *J. Metamorph. Geol.* **4**, 179-199.
- ____ & TILL, A.B. (1987): Possible crustal origin for garnet lherzolite, Kigluaik Mountains, Alaska. *Geol. Soc. Am., Abstr. Programs* **19**(7), 746.
- MATURA, A. (1976): Hypothesen zum Bau und zur geologischen Geschichte des kristallinen Grundgebirges von Südwestmähren und dem Niederösterreichischen Waldviertel. *Jahrb. Geol. B.-A.* **119**, 63-74.
- McMULLIN, D.W., BERMAN, R.G. & GREENWOOD, H.J. (1991): Calibration of the SGAM thermobarometer for pelitic rocks using data from phase-equilibrium experiments and natural assemblages. *Can. Mineral.* **29**, 889-908.
- PATRICK, B.E. & EVANS, B.W. (1989): Metamorphic evolution of the Seward Peninsula blueschist terrane. *J. Petrol.* **30**, 531-555.
- ____ & LIEBERMAN, J.E. (1988): Thermal overprint on blueschists of the Seward Peninsula: the Lepontine in Alaska. *Geology* **16**, 1100-1103.
- PETRAKAKIS, K. (1986): Metamorphism of high grade gneisses from the Moldanubian Zone, Austria, with particular reference to the garnets. *J. Metamorph. Geol.* **4**, 323-344.
- ____ & DIETRICH, H. (1985): MINSORT: a program for the processing and archiving of microprobe analyses of silicate and oxide minerals. *Neues Jahrb. Mineral. Abh.* **8**, 379-384.
- ____ & RICHTER, W. (1990): Gföhler Gneise und Granulite aus dem mittleren und südlichen NÖ-Moldanubikum. *Österr. Beitr. Meteor. Geoph.*, in press.
- POWELL, R. (1985): Geothermometry and geobarometry: a discussion. *J. Geol. Soc. Lond.* **142**, 29-38.
- ROCK, N.M.S. (1988): *Numerical Geology: a Source Guide, Glossary, and Selective Bibliography to Geological Uses of Computers and Statistics*. Springer-Verlag, Heidelberg, Germany.
- RODDICK, J.C. (1987): Generalized numerical error analysis with applications to geochronology and thermodynamics. *Geochim. Cosmochim. Acta* **51**, 2129-2135.
- RUBINSTEIN, R.Y. (1981): *Simulation and the Monte Carlo Method*. J. Wiley and Sons, New York.
- SCHARBERT, G.H. & CARSWELL, D.A. (1983): Petrology of garnet-clinopyroxene rocks in a granulite facies environment, Bohemian massif of Lower Austria. *Bull. Minéral.* **106**, 761-774.
- ____ & KURAT, G. (1974): Distribution of some elements between coexisting ferromagnesian

- minerals in Moldanubian granulite facies rocks, Lower Austria, Austria. *Tschermaks Mineral. Petrogr. Mitt.* **21**, 110-134.
- THIELE, O. (1976): Ein westvergenger kaledonischer Deckenbau im Niederösterreichischen Waldviertel? *Jahrb. Geol. B.-A.* **119**, 75-81.
- _____ (1984): Zum Deckenbau und Achsenplan des Moldanubikums der Südlichen Böhmisches Masse (Österreich). *Jahrb. Geol. B.-A.* **126**, 513-523.
- TILL, A.B. (1980): *Crystalline Rocks of the Kigluaik Mountains, Seward Peninsula, Alaska*. M.S. thesis, Univ. Washington, Seattle, Washington.
- _____, DUMOULIN, J.A., GAMBLE, B., KAUFMAN, D. & CARROL, P.I. (1986): Preliminary geologic map and fossil data, Solomon, Bendeleben and Southern Kotzebue quadrangles, Seward Peninsula Alaska. *U.S. Geol. Surv., Open-File Rep.*
- TODD, C. & EVANS, B.W. (1990): Isotopic and petrologic evidence for limited fluid infiltration during granulite grade metamorphism in the Kigluaik Mountains, Seward Peninsula, AK. *Geol. Soc. Am., Abstr. Programs* **22(7)**, A259.
- TOLLMANN, A. (1982): Grossräumiger variszischer Deckenbau im Moldanubikum und neue Gedanken zum Variszikum Europa. *Geotektonische Forschung* **64**, 91.
- _____ (1985): *Geologie von Österreich 2*. Deuticke, Vienna, Austria.
- VAN BREEMEN, O., AFTALION, M., BOWES, D.R., DUDEK, A., MISAR, Z., PORONDRA, P. & VRANA, S. (1982): Geochronological studies of the Bohemian Massif, Czechoslovakia, and their significance in the evolution of central Europe. *Trans. Roy. Soc. Edinburgh, Earth Sci.* **73**, 89-108.

Received January 21, 1991, revised manuscript accepted October 5, 1991.